Supplementary Materials for

Field-deployable viral diagnostics using CRISPR-Cas13

Cameron Myhrvold,* Catherine A. Freije,* Jonathan S. Gootenberg, Omar O. Abudayyeh, Hayden C. Metsky, Ann F. Durbin, Max J. Kellner, Amanda L. Tan, Lauren M. Paul, Leda A. Parham, Kimberly F. Garcia, Kayla G. Barnes, Bridget Chak, Adriano Mondini, Mauricio L. Nogueira, Sharon Isern, Scott F. Michael, Ivette Lorenzana, Nathan L. Yozwiak, Bronwyn L. MacInnis, Irene Bosch, Lee Gehrke, Feng Zhang, and Pardis C. Sabeti*

*correspondence to: pardis@broadinstitute.org (P.C.S.); cmyhrvol@broadinstitute.org (C.M.); cfreije@broadinstitute.org (C.A.F.)

This PDF file includes:

Materials and Methods

Clinical samples / ethics statement

Clinical samples used for this study were from clinical studies evaluated and approved by the Institutional Review Boards/Ethics Review Committees at Hospital General de la Plaza de la Salud (Santo Domingo, Dominican Republic), Florida Department of Health (Tallahassee, Florida), and Universidad Nacional Autonoma de Honduras (Tegucigalpa, Honduras). Massachusetts Institute of Technology (MIT) Institutional Review Board/Ethics Review Committee and the Office of Research Subject Projection at the Broad Institute provided approval for use of samples collected by the previously listed institutions. For the dengue virus clinical samples, The Broad Institute Institutional Review Board/Ethics Review Committee provided approval for the use of the samples. The specific sample aliquots we tested in this paper cannot be shared due to MTA restrictions. Additional clinical samples from similar patients can be obtained either commercially (samples from Boca Biolistics) or by contacting the corresponding authors.

Zika virus (ZIKV) clinical samples were collected during the 2015-2016 ZIKV pandemic and tested at collaborating sites with either the Hologic Aptima ZIKV assay, or published ZIKV RT-PCR or RT-qPCR assays depending on the collaborating site. The nucleic acid testing and results are reported in Table S1. Extracted RNA from these collected clinical samples were prepared for metagenomic and targeted sequencing and genomes published previously(*3*) and cDNA from these 40 preparations were used as input for comparing SHERLOCK to amplicon PCR performance. Extracted RNA from 16 of these samples were also tested using the Altona RealStar Zika virus RT-PCR kit, details of the assay are found below and the samples tested and their results are reported in Table S2.

Confirmed positive dengue virus (DENV) patient serum samples were excess from the comparative genomics of DENV for the Broad Institute Viral Genomics Initiative. In addition, four confirmed DENV positive patient serum samples and three matched saliva samples were obtained from Boca Biolistics. Extracted RNA from DENV RT-PCR positive human serum samples, and clinical isolates were excess from the comparative genomics of DENV for the Broad Institute Viral Genomics Initiative. Clinical isolates were prepared by culturing human serum on C6/36 cells and harvesting RNA from the cell supernatant with the RNA extraction protocol outlined below.

Production of LwCas13a and crRNAs

LwCas13a was purified as described in-house(*13*) or by Genscript. crRNA DNA templates were annealed to a T7 promoter oligonucleotide at a final concentration of 10 μM in 1x Taq reaction buffer (NEB). This involved 5 minutes of denaturation at 95 °C followed by an anneal at 5 °C per minute down to 4 °C. crRNAs were transcribed in vitro using the HiScribe T7 High Yield RNA Synthesis Kit (NEB). Transcriptions were performed according to the manufacturer's instructions for short RNA transcripts, with the volume scaled to 30 μl. Reactions were incubated overnight at 37 °C. Transcripts were purified using RNAClean XP beads (Beckman Coulter) with a 2x ratio of beads to reaction volume and an additional supplementation of 1.8x isopropanol. Some crRNAs were synthesized by Integrated DNA Technologies (IDT).

Sample preparation

Viral RNA was extracted from 140 µl of input material using the QIAamp Viral RNA Mini Kit (QIAGEN) with carrier RNA according to the manufacturer's instructions. Samples were eluted in 60 µl of nuclease free water and stored at -80 °C until use.

To produce cDNA, 5 µl of extracted RNA was converted into single-stranded cDNA using methods published previously(*27*). In short, RNA was reverse transcribed with SuperScript III (Invitrogen) and random hexamer primers. RNA-DNA duplexes were then degraded with RNase H. cDNA was stored at -20 °C until use. In some experiments (Fig. 1C, Fig. S3), reverse transcription was performed using SuperScript IV for 20 minutes at 55 °C, without RNase H treatment.

A single cultured isolate, ZIKV Pernambuco (isolate PE243, KX197192.1), was used as a positive control or as a control for the ancestral sequence in ZIKV detection experiments. Viral RNA was extracted from 140 µl of the seed stock sample using the RNA extraction method described above.

RNase inactivation of urine samples was performed by addition of TCEP/EDTA and heating samples. TCEP and EDTA were added to urine samples at final concentrations of 100 mM and 1 mM respectively. Two protocols were used: 1-step inactivation at 95 °C for 10 minutes, or 2-step inactivation at 50 °C for 20 minutes followed by 95 °C for 5 minutes. Inactivations were performed using a thermocycler or a dry heat block.

RNase inactivation of ZIKV in whole blood, plasma, serum, and saliva samples was performed by addition of TCEP/EDTA and heating samples. TCEP and EDTA were added to urine samples at final concentrations of 100 mM and 1 mM respectively. A 2-step inactivation at 50 °C for 5 minutes followed by 64 °C for 5 minutes (blood products or saliva), or 50 °C for 20 minutes followed by 95 °C for 5 minutes (urine) was used. Inactivations were performed using a thermocycler or a dry heat block.

RNase inactivation of DENV in whole blood, serum, and saliva samples was performed by addition of TCEP/EDTA and heating samples. TCEP and EDTA were added to urine samples at final concentrations of 100 mM and 1 mM respectively. A 2-step inactivation at 42 °C (or in some experiments, 37 °C) for 20 minutes followed by 64 °C for 5 minutes was used. Inactivations were performed using a thermocycler.

RPA reactions and primer design

For RPA reactions, the Twist-Dx RT-RPA kit was used according to the manufacturer's instructions. Primer concentrations were 480 nM. For amplification reactions involving RNA, Murine RNase inhibitor (NEB M3014L) was used at a final concentration of 2 units per microliter. All RPA reactions were 20 minutes unless otherwise stated.

For ZIKV detection, RPA primers RP819/RP821 from a recent publication were used(*13*). For pan-DENV detection, irrespective of serotype, an equal mix of published RPA primers DENV1-3-RPA-RP4/DENV1-3-RPA-FP13 and DENV4-RPA-RP2/DENV4-RPA-FP3 were used(*28*).For the flavivirus panel, RPA primers FLAVI-NS5fwd-1/FLAVI-NS5rev-1 were used. For the DENV panel to differentiate between serotypes, RPA primers DENV-3UTRfwd-1/DENV-3UTRrev-1 were used. For region-specific ZIKV SNP detection, RPA primers DOMUSA-5249-fwd / DOMUSA-5249-rev

(DOMUSA5249 SNP), USA-935-fwd / USA-935-rev (USA935 SNP), and HND-2788-fwd / HND-2788-rev (HND2788 SNP) were used. For detecting a ZIKV SNP associated with microcephaly, RPA primers ZIKV-mcep-fwd and ZIKV-mcep-rev were used. For detecting drug-resistance SNPs in HIV reverse transcriptase, RPA primers HIVRT-149F / HIVRT-348R (K65R, K103N, and V106M SNPs), and HIV-462F / HIVRT-601R (Y181C, M184V, and G190A SNPs) were used. For a complete list of RPA primer names and sequences, see Table S5.

Cas13 detection reactions and crRNA design

Detection reactions were performed as described(*13*), except that background RNA input per reaction was reduced from 100 to 0-25 ng. This increases the reaction rate without introducing any spurious cleavage of the reporter oligonucleotide. Unless indicated otherwise, RNase Alert v2 (Thermo) was used as the reporter. Biotek microplate readers (Synergy H4, Neo2, and Cytation 5) were used for measuring fluorescence of the detection reaction. Fluorescence kinetics were monitored using a monochromator with excitation at 485 nm and emission at 520 nm with a reading every 5 minutes for up to 3 hours. We did not observe significant differences in sensitivity between the different machines; machines were thus utilized interchangeably. Fluorescence values reported were background subtracted or template-specific values. Time point reported is 1 hour unless otherwise stated.

For ZIKV detection, the crRNA "Zika targeting crRNA 2" from a recent publication was used*(13*). For pan-DENV detection irrespective of serotype, a equal mix of 3 crRNAs and D1-3UTRat10660, D2/3-3UTRat10635, D4-3UTRat10620 were used. For the flavivirus panel, crRNAs ZIKV-NS5at9227 (ZIKV), DENV-NS5at9127 (DENV), WNV-NS5at9243 (WNV), and YFV-NS5at9122 (YFV) were used. For the DENV panel to differentiate between serotypes, crRNAs D1-3UTRat10457 (DENV1), D2-3UTRat10433 (DENV2), D3-3UTRat10419 (DENV3), and D4-3UTRat10366 (DENV4) were used. For region-specific ZIKV SNP detection, crRNAs DOMUSA-5249-ancestral / DOMUSA-5249-derived (DOMUSA5249 SNP), USA-935-ancestral / USA-935-derived (USA935 SNP), and HND-2788-ancestral / HND-2788-derived (HND2788 SNP) were used. For detecting a ZIKV SNP associated with microcephaly, crRNAs ZIKV-mcep-snp3syn5-ancestral / ZIKV-mcep-snp3syn5-derived (design shown in Fig. 4F), and crRNAs ZIKV-mcep-snp7-ancestral / ZIKV-mcep-snp7-derived (design shown in Fig. S11) were used. For detecting drug-resistance SNPs in HIV reverse transcriptase, crRNAs HIVRT-K65R-ancestral / HIVRT-K65R-derived (K65R SNP), HIVRT-K103N-ancestral / HIVRT-K103N-derived (K103N SNP), HIVRT-V016M-ancestral / HIVRT-V106M-derived (V106M SNP), HIVRT-Y181C-ancestral / HIVRT-Y181C-derived (Y181C SNP), HIVRT-M184V-ancestral / HIVRT-M184V-derived (M184V SNP), and HIVRT-G190A-ancestral / HIVRT-G190A-derived (G190A SNP) were used. For a complete list of crRNA names and spacer sequences, see Table S6. For additional discussion of the effect of crRNA sequence and secondary structure on activity, see the supplementary text.

Lateral flow detection reactions

Lateral flow detection was achieved using a custom probe oligonucleotide (LF-polyU, see Table S7 for the sequence) with commercially available detection strips

(Milenia Hybridetect 1, TwistDx, Cambridge, UK). Cas13 detection reactions were diluted 1:5 in Hybridetect Assay Buffer, then the strips were inserted and incubated for 5 minutes at room temperature. The strips were then removed and photographed using a smartphone camera.

RT-PCR experiments

RT-PCR for ZIKV detection was performed using the Altona RealStar Zika Virus RT-PCR Kit (RUO version) according to the manufacturer's specifications on a Lightcycler 96 RT-PCR machine (Roche). Ten µl of ZIKV RNA extracted from patient samples was used as an input for RT-PCR. One µl of internal control (IC) was used for each sample.

Data analysis

Background subtraction was performed by subtracting the fluorescence values after 0 minutes (Figs. 1D, S1, S6-S7), 10 minutes (Figs. 1B-C, 2, 3, and associated supplemental figures) or 20 minutes (Fig. 4 and associated supplemental figures), when minimum fluorescence was observed. For both the flavivirus panel and the DENV panel, background subtracted fluorescence was normalized to target-specific fluorescence. Target specific fluorescence is the mean background subtracted fluorescence of the no input (water) control with a given crRNA subtracted from the background subtracted fluorescence of a given target with the same crRNA at each time point.

For the analysis of ZIKV samples from the 2015-2016 pandemic (Fig. 1B), thresholds were used to determine the presence or absence of ZIKV. The ZIKV SHERLOCK fluorescence threshold was determined using background subtracted fluorescence from 5 negative control samples: 4 single-donor healthy human urine samples and one no-input water control. Namely, for each sample *s* of these 5, we took the mean m_s and standard deviation σ_s of the fluorescence across 3 technical replicates. The threshold was set to the median of the 5 values $\{m_s+3\sigma_s\}$. For Fig. 1C, the same calculation $\{m_s+3\sigma_s\}$ was performed using 1 no input control to determine the threshold. The threshold on amplicon PCR yield was determined using information from genome assemblies. First, the amplicon PCR yield was calculated for each sample by taking the minimum concentration from each of the two amplicon PCR pools (Fig. S2A). The objective is then to determine a yield that best predicts whether a particular targeted portion *r* of the genome is present in a sample (in this case, the RPA amplicon we are detecting with SHERLOCK). The probability that *r* is present in a sample *s*, $Pr_s(r)$, can be estimated as the fraction of the ZIKV genome that was sequenced and assembled from cDNA of *s*. (Calculating a probability across the genome is preferable to simply looking at whether there is coverage in the genome at *r* because lack of coverage does not necessarily indicate that *r* is not present.) The data for this analysis are from individual technical replicates from a recent genome sequencing study of the ZIKV pandemic(*3*). A plot of amplicon PCR yield vs. fraction of the genome covered is shown in Fig. S4B. The values $Pr_s(r)$ can be used to estimate precision and recall for a choice of threshold. In particular, an estimate of the number of samples that do have *r* is the sum of $Pr_s(r)$ across all samples. Similarly, among the samples *P* whose amplicon PCR yield exceeds a given threshold, the number that are correctly labeled as having presence of *r* is estimated as the sum of $Pr_s(r)$ across the samples in *P*. Fig. S2C shows precision and recall for each

choice of threshold, as well as the the $F_{0.5}$ score, which is a composite metric that takes into account the threshold's ability to accurately classify samples as having the targeted portion of ZIKV. The amplicon PCR yield threshold was set to maximize the $F_{0.5}$ score. For additional discussion of the sensitivity and specificity of SHERLOCK compared to amplicon PCR and other methods, see the supplementary text.

DENV SHERLOCK fluorescence threshold was calculated similar to described above with the ZIKV assay. Background subtracted fluorescence from 8 no input negative controls were used to determine the threshold. For each no input control *s* of these 8, we took the mean m_s and standard deviation σ_s of the fluorescence across 3 technical replicates and the threshold was set to the median of the 8 values $\{m_s+3\sigma_s\}$.

For multivirus or serotype panels, we calculated off-target fluorescence for each target against the other crRNAs in the panel. This was performed by calculating the percentage of target-specific fluorescence for an unmatched target:crRNA pair relative to the target-specific fluorescence observed for the matching target:crRNA pair at the 3 hour detection time point (when maximum fluorescence was observed or signal had saturated). Off-target fluorescence reported in the text was the maximum observed for the 4 targets in a given panel.

For SNP identification, background subtracted fluorescence values were calculated using ancestral-targeting and derived-targeting crRNAs. We took the ratio of the derived background-subtracted fluorescence to the ancestral background-subtracted fluorescence to determine the presence or absence of a SNP. For the HIV SNPs (Fig. S12), we calculated the SNP identification index, which is the ratio of the fluorescence ratio for the derived allele divided by the fluorescence ratio for the ancestral allele. The SNP identification index is equal to 1 if there is no discriminatory power between the two alleles, and increases as the fluorescence ratios between the two alleles diverge. For additional discussion of the factors influencing the ease of differentiating individual SNPs using SHERLOCK, see the supplementary text.

ZIKV and DENV detection experiments

PE243 (KX197192.1) seedstock cDNA was used at a stock concentration of 6.8 x 10^4 cp/µl. cDNA was serially diluted 1:10 in ultrapure water (Life Technologies), or healthy urine (Lee Biosolutions). 4-8 µl of each sample was inactivated, and 1-2 µl was used as input for RPA reactions. PE243 seedstock RNA was used at 2.72 x 10^5 cp/µl. The virus was originally isolated from a febrile patient with rash on May 13th, 2015, and Vero cell passages were done at the FIOCRUZ Pernambuco laboratory (E. Marques), in Brazil in 2016 and at MIT Gehrke laboratory. PE243 is one of the first isolates from the ZIKV pandemic in Brazil(*29*). RNA was serially diluted 1:10 in ultrapure water (Life Technologies), or healthy urine (Lee Biosolutions). 4-8 µl of each sample was inactivated, and 1-2 µl was used as input for RPA reactions. We used 14 mM MgAc for DENV detection and 17 mM MgAc for ZIKV detection.

A cultured isolate, ZIKV strain PRVABC59 (KU501215) from Puerto Rico(*29,30*) was acquired through the BEI repository in USA cat number ATCC VR-1843 and used for addition of virus to healthy urine, saliva, whole blood, and serum samples. PRVABC59 was cultured in insect and non-human primate cell lines. HuH-7 human hepatoma cells were used for deriving the infectious particles in the virus stock as described(*31*). A cultured isolate, DENV2 strain New Guinea C (NGC) was used for

dilution of virus in healthy saliva (Lee Biosolutions), whole blood (Research Blood Components), and serum (Millipore Sigma).

Viral panel experiments

In order to account for the sequence diversity between 4 different viruses in the flavivirus family (ZIKV, DENV, WNV, and YFV), we applied the method CATCH (Compact Aggregation of Targets for Comprehensive Hybridization) to search for conserved regions that would be suitable for a pan-flavivirus RPA primer pair. An implementation of this method is available on GitHub under the MIT license (https://github.com/broadinstitute/catch). This method allowed us to narrow our search for primer pairs within a conserved region of NS5.

For initial testing of the flavivirus panel and DENV panel, synthetically derived DNA templates were used as input at a concentration of 10^4 copies/µl. A no input (water) control was used as a negative control for each of the crRNAs tested. In all panel experiments, 3 technical replicates were used. In all flavivirus panel experiments, the MgAc concentration in the RPA reaction was 20 mM while in all DENV panel experiments MgAc concentration in the RPA was 14 mM.

For initial testing of the flavivirus panel, ZIKV template sequence was derived from (KX197192.1), DENV (NC_001477.1), WNV (NC_09942.1), and YFV (AY968065.1). The RPA reaction amplifies a portion of NS5 for these flaviviruses.

For initial testing of the DENV panel, the DENV1 synthetic template sequence was derived from (KM204119.1), DENV2 (KM204118.1), DENV3 (KU050695.1), DENV4 (JQ822247.1). The RPA reaction amplifies a portion of the 3'UTR region of DENV1-4. The DENV panel was additionally tested on extracted RNA from clinical samples and seed stocks.

SNP identification experiments

For region-specific SNP identification, synthetic templates containing 400-nt fragments of the ZIKV genome with ancestral or derived alleles were used to validate the performance of the SNP identification assay. In addition, ZIKV cDNA samples from 3 countries (USA, Honduras, and Dominican Republic) were used to confirm performance on mosquito pools and clinical samples. See Table S1 for additional information about these cDNA samples. PE243 seedstock cDNA (KX197192.1) was used as an outgroup control at 300 cp/µl. In addition, a no input (water) control was used. For the microcephaly-associated SNP identification experiments, synthetic templates containing a 400-nt fragment of the ZIKV genome with ancestral or derived alleles were used at 10^4 cp/µl, and PE243 seedstock cDNA was used at 300 cp/µl. For the HIV drug resistance SNP identification experiments, synthetic templates containing 468-nt fragments of the HIV genome with ancestral or derived alleles were used at 10^4 cp/µl. For a complete list of synthetic template names and sequences, see Table S7. In all SNP identification experiments, 3 technical replicates were used.

Supplementary Text

Discussion of the sensitivity and specificity of SHERLOCK for ZIKV detection

We have shown that SHERLOCK is a very sensitive and specific method for nucleic acid detection. ZIKV detection was a key test of SHERLOCK's sensitivity, in large part

because the ZIKV is notoriously challenging to detect due to low viral titers and sample degradation(*2*). We tested a set of 37 suspected positive patient samples and 3 mosquito pools from the 2015-16 ZIKV pandemic with both SHERLOCK and amplicon PCR to determine the presence or absence of ZIKV nucleic acid in a given sample. For 16 samples from these patient, we were able to compare SHERLOCK to two FDA-EUA-approved ZIKV diagnostics: 1) Hologic Aptima ZIKV assay, and 2) Altona RealStar Zika Virus RT-PCR assay.

To compare SHERLOCK and the Altona RealStar Zika Virus RT-PCR assay, we compared both assays on a set of 16 patient samples. We performed the two assays such that the reverse transcription conditions and input volumes were equivalent: 20 minute reverse transcription and 10 µl input. cDNA is diluted 1:4 from the RNA input due to the reverse transcription reaction conditions, thus the amount of RNA that we are using for SHERLOCK is ¼ the amount used by the Altona kit. We observed equal sensitivity between the two methods, with 10 of 16 samples positive by each method and 100% concordance overall (Figs. 1C, S3).

We then compared SHERLOCK and the Altona assay to the Hologic Aptima Zika Virus Assay, which uses a much larger input volume (> 500 µl). All 10 samples positive by both the Altona assay and SHERLOCK were positive by the Hologic assay (Table S2). Three samples were positive by the Hologic assay but not the other two assays, likely due to the >50x larger sample input volume for the Hologic assay. In conclusion, SHERLOCK has equivalent sensitivity to RT-PCR assays for ZIKV detection, and its sensitivity relative to the Hologic assay is limited by the input volume.

Our rationale for including amplicon PCR data was based on our observations while performing wide-scale genome sequencing during the ZIKV pandemic(*3*) that partial genomes were very common. This suggested that a genome-wide comparator would offer higher sensitivity than single-amplicon approaches such as RT-PCR. With the amplicon PCR approach, we quantified the amplicon PCR products using an Agilent tapestation and selected a threshold of 2 ng/µl for determining the presence or absence of ZIKV, which maximizes accuracy as measured by genome sequence coverage of the amplicon PCR product (Fig. S3, see Methods for details). There was high concordance (82.5%) between the two methods despite differences between the regions of the ZIKV genome they target (Fig. S4). The amplicon PCR method tiles the entire ZIKV genome, whereas SHERLOCK uses only one amplicon that at 128 nt long is shorter than the 300-400 nt long PCR amplicons (Fig. S5). Thus, it is possible for highly degraded samples (with short RNA fragments) to be more readily detected by SHERLOCK than by amplicon PCR. Conversely, if the SHERLOCK amplicon itself has degraded but other parts of the genome have not, then amplicon PCR will detect the remaining portions of the genome present in a sample.

This sensitivity of SHERLOCK is paired with high specificity. We have shown SNP-sensitivity, serotype identification, and species-level specificity using various SHERLOCK assays. We have also tested numerous negative controls, including healthy bodily fluids, water, and in some cases nucleic acid from other viruses. Based on these results, we do not expect to observe many false-positives (if any) using SHERLOCK.

Causes of variability in SHERLOCK performance

As discussed in the supplementary text of the original SHERLOCK paper, RPA performance is highly variable and depends on the template sequence, amplicon length, and other factors(*13*). The Cas13 detection step amplifies fluorescent signals by a factor of 100 to 1,000 or more, depending on the input concentration of the RPA amplicon. As a result, SHERLOCK is fairly robust to variation in either RPA amplification or Cas13 detection, unless this variation is very large in magnitude.

To design multivirus and multi-serotype panels, we used degenerate RPA primers to capture the remarkable sequence diversity of related RNA viruses. In some cases, primer degeneracy can lead to variable amplification efficiency for different targets. In general, this can be managed by optimizing the RPA reaction (adjusting primer and magnesium concentrations, etc.).

In addition to RPA variation, we have observed some variation in the Cas13 detection step of SHERLOCK due to the effects of spacer GC content, stretches of polyUs, and secondary structure on crRNA performance. Some crRNAs are more active than others, and some crRNAs show more activity in absence of target (i.e. no input controls). We have also observed that some crRNAs are less pure than others after *in vitro* transcription. After purification, however, almost all crRNAs are highly active (with a few exceptions due to undesirable secondary structure of the spacers, such as when most of the spacer can pair with itself).

The lower ZIKV fluorescence in the flavivirus panel (Fig. 3B) may be due a combination of the factors discussed above (likewise for other crRNAs used in this study).

<u>Factors influencing SNP discrimination by SHERLOCK</u>

Different spacer RNA sequences were observed to have different levels of performance in the detection step of SHERLOCK. Factors that lead to these differences in performance were discussed above, but there are also implications related to SNP detection.

SNP detection relies on a pair of crRNAs that differ from a target sequence by one or two nucleotides, and thus have differential activity on a target molecule that is sequence-dependent. SNP discrimination is successful when the presence of a 2nd mismatch between the crRNA and target RNA leads to observable differences in collateral cleavage. Therefore, the following could limit the success of SNP discrimination:

- A single additional mismatch in a highly active crRNA may not reduce activity sufficiently for strong discrimination and has been observed for some crRNAs. Possible solutions include 1) diluting the RPA product prior to addition to the detection reaction, or 2) using a lower crRNA concentration.
- If one allele amplifies preferentially to the other during the RPA (due to a change in the secondary structure of the template), this could bias the output of SHERLOCK. We have not observed this, but it is a possibility.
- Wobble pairing of RNA will allow for some crRNAs to bind weakly in the absence of Watson-Crick base pairing. This has been observed for some of our A->G or G->A mutations (e.g. USA935). A “U” in the crRNA can bind to either the derived or ancestral nucleotide. However, even in this scenario it is easy to

distinguish the two alleles as the G-targeting crRNA will contain a C nucleotide, which will not pair with A.

Given these limitations, crRNAs with lower activity (which can be achieved by shortening the spacer) could be better suited for SNP detection, and although wobble base pairing can have an effect on SHERLOCK's signal it will not completely abolish SNP identification.

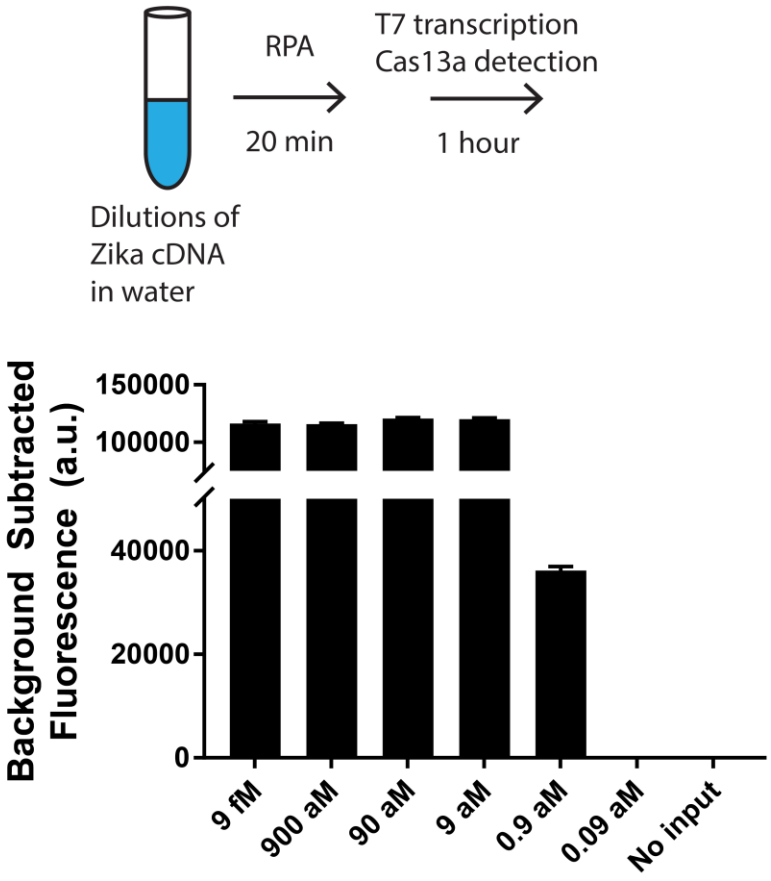

Fig. S1. SHERLOCK can detect Zika virus cDNA with high sensitivity.
We show SHERLOCK fluorescence values after 20 minutes of RPA and 1 hour of detection for serial dilutions of ZIKV cDNA. Sensitivity of 0.9 aM is equivalent to single copy sensitivity as 2 aM = 1 cp/µl and 2 µl of sample was used as input. Error bars indicate 1 S.D. based on 3 technical replicates.

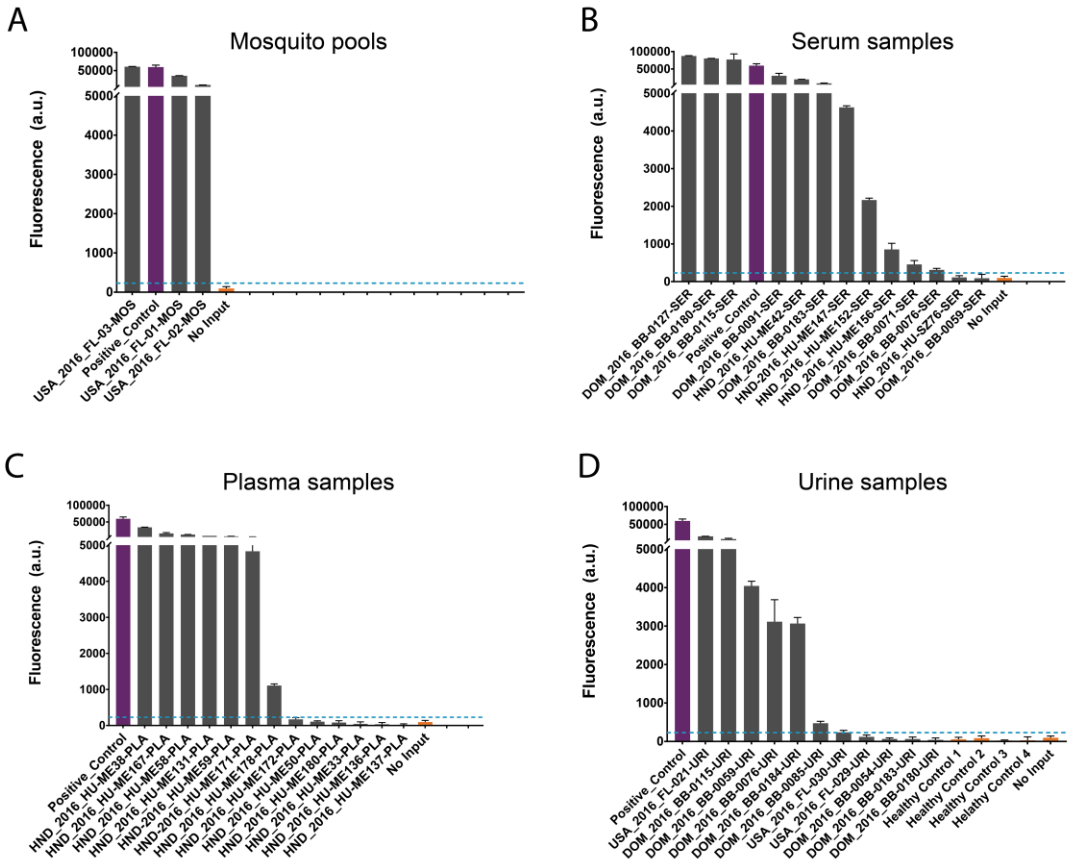

Fig. S2. SHERLOCK fluorescence data for 40 samples from the 2015-2016 Zika virus pandemic.

(A-D) Fluorescence data at 1 hour for 40 cDNA samples. Sample names indicate country of origin, sample collection year, followed by the sample name and sample type. Sample types are as indicated: PLA: plasma sample, SER: serum sample, URI: urine sample, MOS: mosquito pool. Countries of origin are indicated using abbreviations: HND: Honduras, DOM: Dominican Republic, USA: United States. Error bars indicate 1 S.D. based on 3 technical replicates. The positive control (purple) shown in each plot is a cultured viral seed stock (PE243). Negative controls are shown in orange.

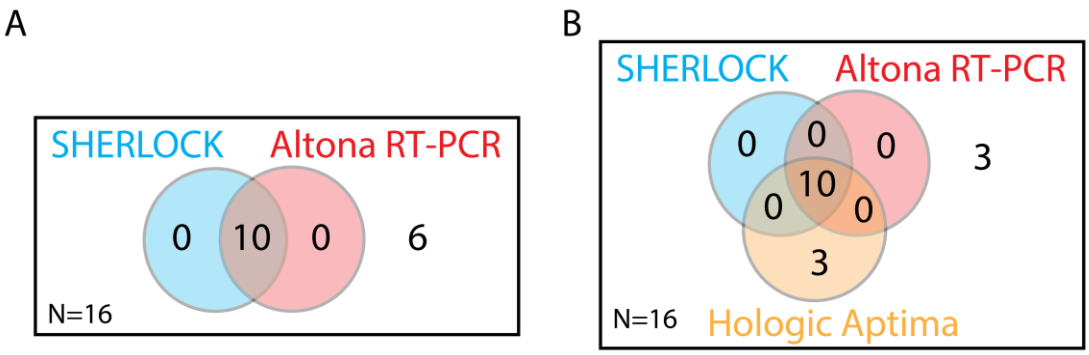

Fig. S3. Comparison between SHERLOCK and other nucleic acid amplification tests.
We show Venn diagrams comparing the results of (A) SHERLOCK vs. the Altona RealStar Zika Virus RT-PCR assay, and (B) SHERLOCK vs. the Altona RealStar Zika Virus RT-PCR assay and the Hologic Aptima Zika Virus assay.

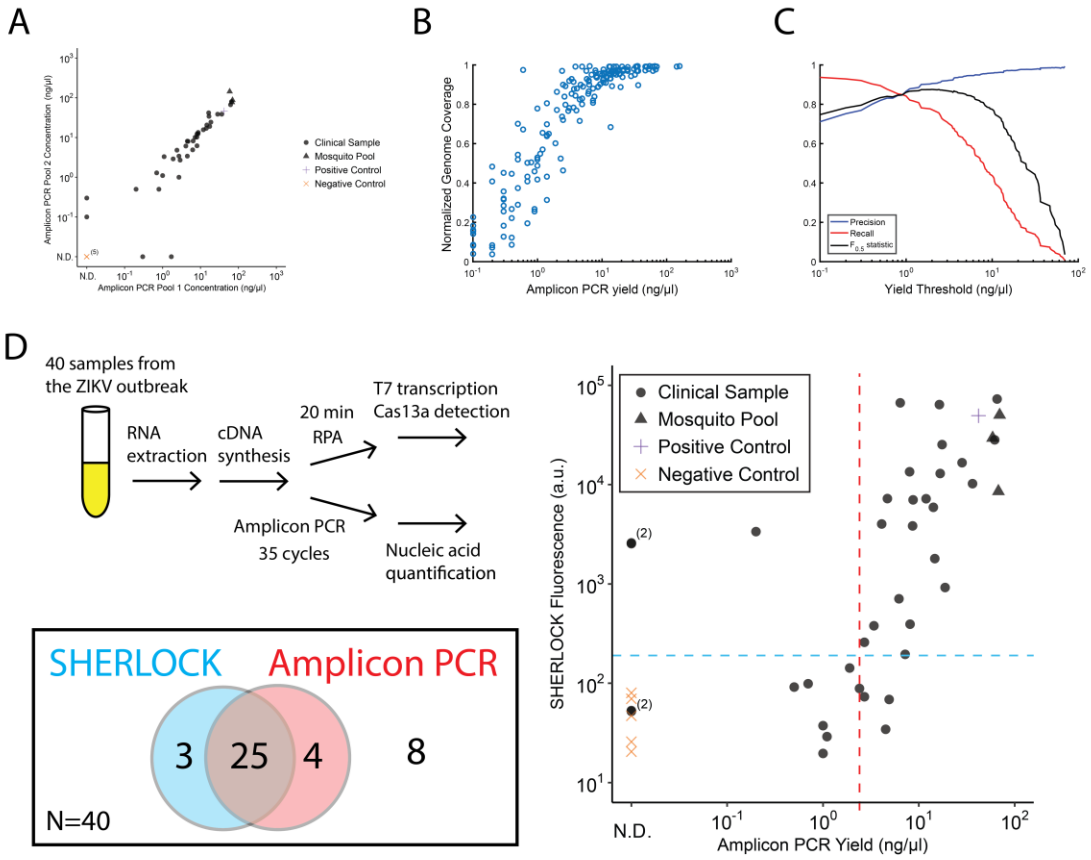

Fig. S4. Comparison of SHERLOCK fluorescence to amplicon PCR yield for the samples from Table S1.
(A) A scatterplot of ng/µl concentrations (measured by Agilent TapeStation) from each of the 2 amplicon PCR primer pools for each cDNA sample. In some cases, data points are nearly superimposed, indicated by a number in parentheses. N.D.: not detected. The positive control (purple cross) is a cultured viral seed stock (PE243) and the negative controls (orange x) include 1 no input control and 4 single donor healthy urine samples. (B) A scatterplot of the amplicon PCR yield (in ng/µl) versus the genome coverage from our recent ZIKV sequencing efforts. The amplicon PCR yield is defined as the minimum amplicon DNA concentration of the two amplicon PCR pools (measured by Agilent tapestation). Genome coverage is normalized to 1. Technical replicates of sequencing libraries are shown as separate circles. (C) We show the precision (true positives divided by the sum of true positives and false positives), recall (sensitivity), and the $F_{0.5}$ statistic for varying amplicon PCR yield thresholds. The threshold for the amplicon PCR yield was selected to maximize the $F_{0.5}$ statistic. (D) Comparison between amplicon PCR yield and SHERLOCK fluorescence. Dashed lines denote thresholds for the presence or absence of ZIKV; blue: SHERLOCK, red: amplicon PCR. The Venn diagram shows the number of samples passing these thresholds for each method. In some cases, data points are nearly superimposed, indicated by a number in parentheses. N.D.: not detected.

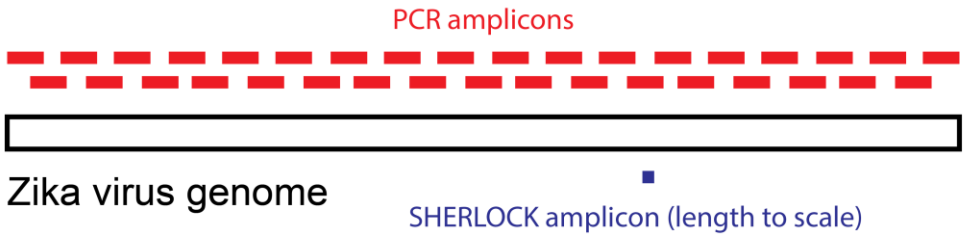

Fig. S5. Schematic of the regions of the Zika virus genome targeted by SHERLOCK and other diagnostic methods.
PCR amplicons tile the entire ZIKV genome, whereas the SHERLOCK ZIKV assay targets just one region of the ZIKV genome with a shorter amplicon. The Altona RealStar RT-PCR assay and Hologic Aptima TMA assay also target individual, short amplicons in the ZIKV genome (the locations and sizes of these amplicons are proprietary and are therefore not shown in the schematic). It is possible to have a clinical sample with highly fragmented RNA which cannot be amplified by the PCR primers (which have a product length ~400 nt). Conversely, it is possible to have a clinical sample with a partial ZIKV genome that does not contain the ~120 nt SHERLOCK amplicon.

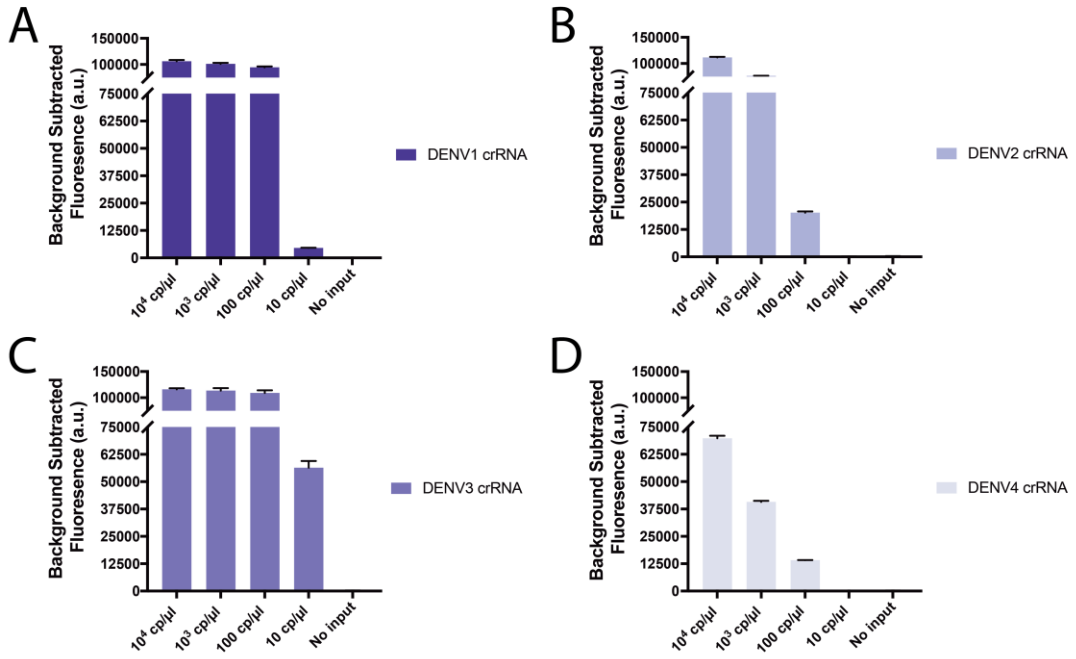

Fig. S6. Limit of detection for pan-dengue SHERLOCK on RNA from 4 dengue virus serotypes.
(A-D) SHERLOCK fluorescence values after 20 minutes of RPA and 1 hour of detection for serial dilutions of DENV RNA derived from a synthetic template. 1 µl of sample was used as input. Error bars indicate 1 S.D. based on 3 technical replicates.

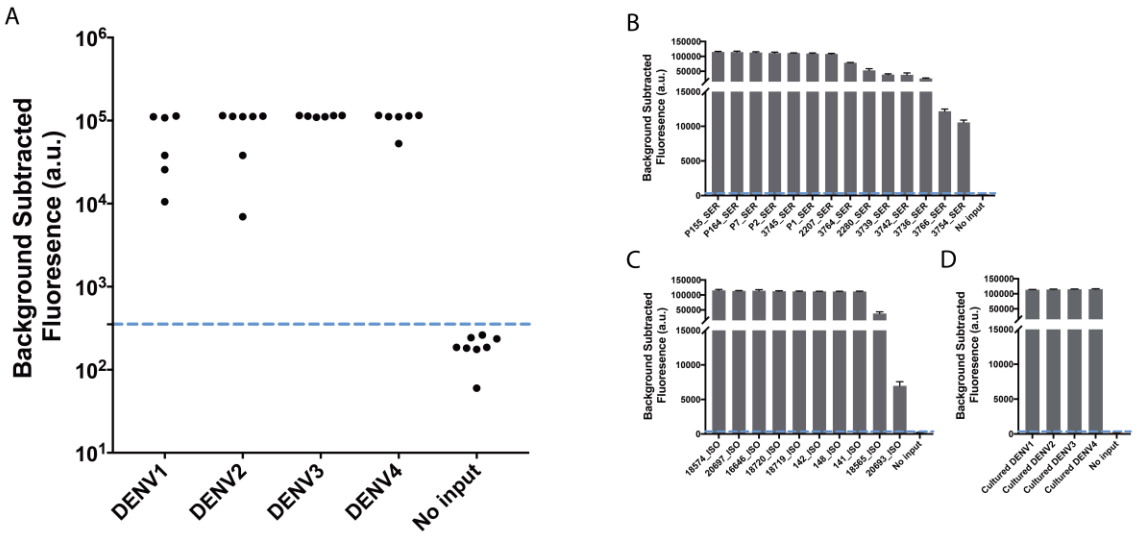

Fig. S7. Pan-dengue SHERLOCK applied to patient samples and clinical isolates. (A) Pan-dengue SHERLOCK fluorescence for RNA extracted from 24 samples and 4 seed stocks denoted by DENV serotype. (B-D) Pan-dengue SHERLOCK fluorescence for RNA extracted from 14 human serum samples at 1 hour of Cas13 detection (B), 10 cultured clinical isolates at 1 hour (C), and 4 DENV seed stocks at 1 hour (D).

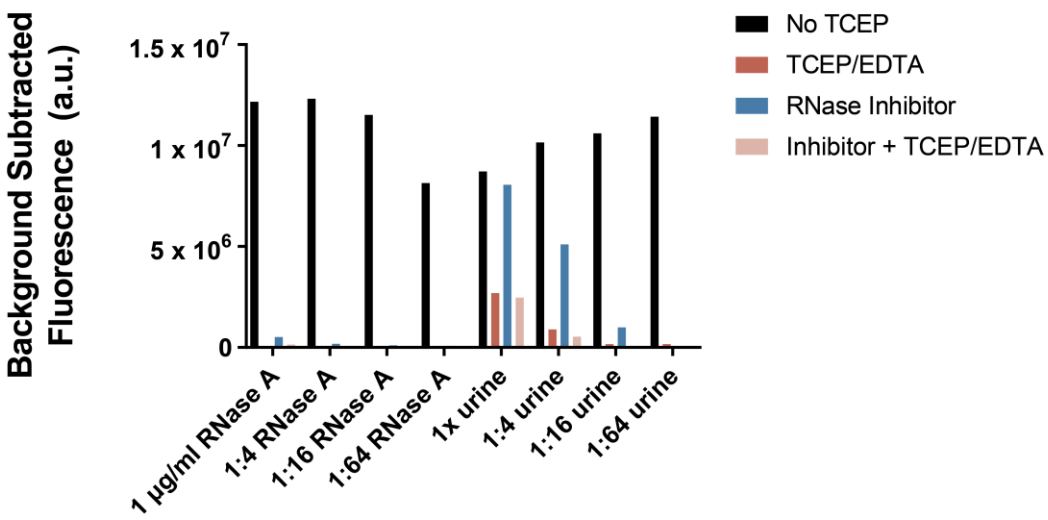

Fig. S8. RNase inactivation using heat and chemical treatment.
Serial 1:4 dilutions of RNase A (1 µg/ml) or healthy human urine were treated with TCEP and EDTA at final concentrations of 100 mM and 1 mM respectively. Samples were incubated at 95 °C for 10 minutes, then RNase Alert v1 (IDT) was added to each sample, and fluorescence was monitored to determine nuclease activity. Fluorescence values are shown after 1 hour of incubation at 37 °C.

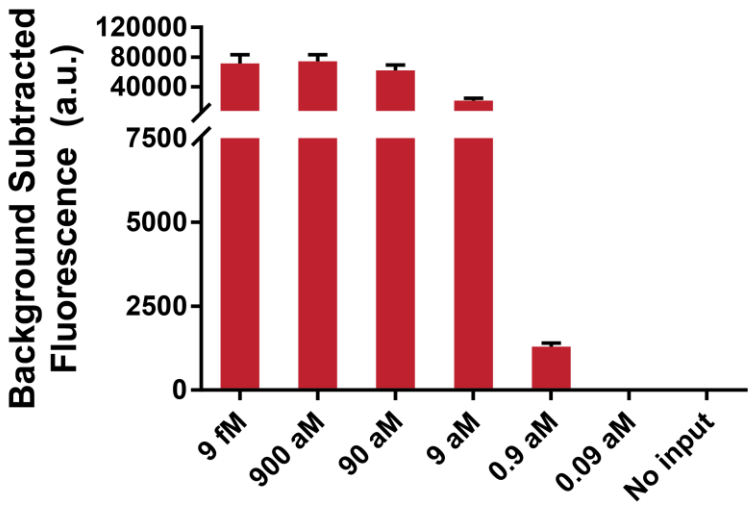

Fig. S9. Detection of Zika virus cDNA directly from urine.
Detection of ZIKV cDNA diluted in healthy human urine (red) using SHERLOCK. Immediately after dilution, urine was treated with TCEP/EDTA and incubated at 95 °C for 10 minutes with 100 mM TCEP and 1 mM EDTA. Error bars indicate 1 S.D. based on 3 technical replicates.

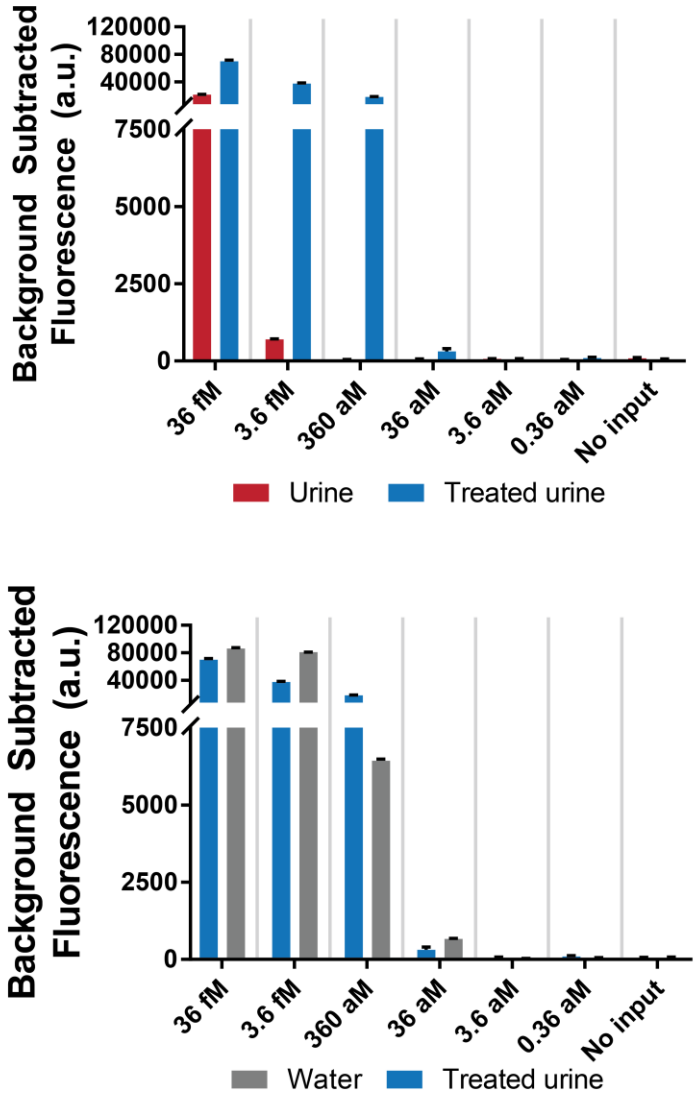

Fig. S10. Detection of Zika virus RNA directly from urine.
Detection of ZIKV RNA diluted in untreated (red) or treated (blue) healthy human urine using SHERLOCK (top). Pretreatment of urine allows for sensitive RNA detection with SHERLOCK. We show fluorescence data after 1 hour of detection for RNA diluted in water (grey), and RNA diluted in urine pre-treated at 95 °C for 10 minutes with 100 mM TCEP and 1 mM EDTA (blue) (bottom).

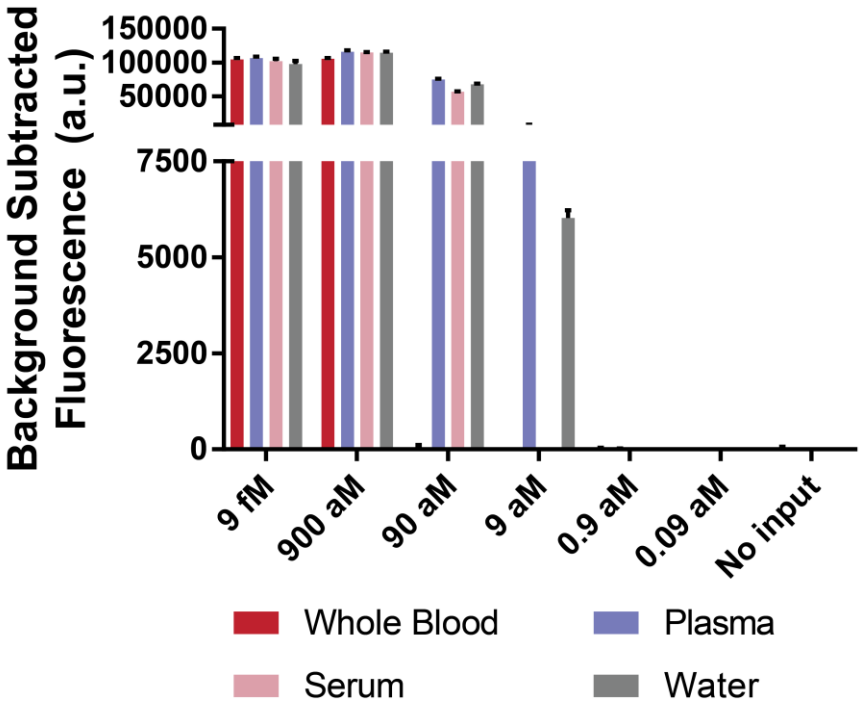

Fig. S11. Detection of Zika virus cDNA directly from blood products.
Detection of ZIKV cDNA diluted in healthy human whole blood (red), healthy human plasma (purple), healthy human serum (pink) or water (grey) using SHERLOCK. Immediately after dilution, bodily fluids were treated at 50 °C for 5 minutes, followed by 64 °C for 5 minutes with 100 mM TCEP and 1 mM EDTA. Error bars indicate 1 S.D. based on 3 technical replicates.

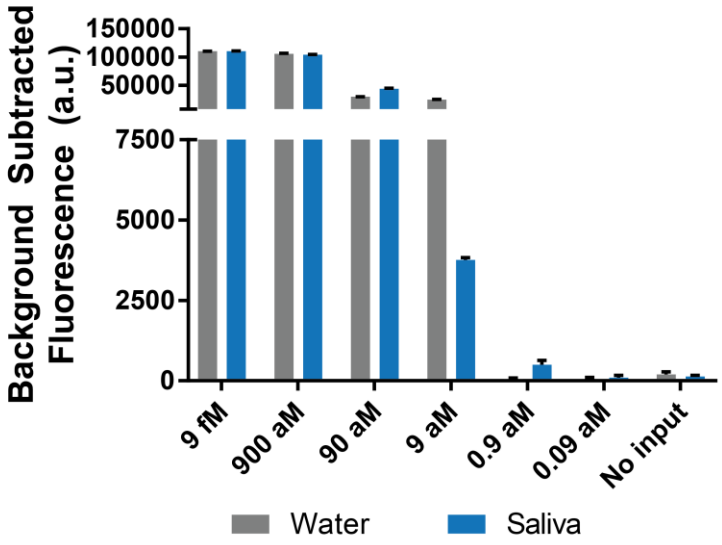

Fig. S12. Detection of Zika virus cDNA directly from saliva.
Detection of ZIKV cDNA diluted in healthy human saliva (blue) or water (grey) using SHERLOCK. Immediately after dilution, bodily fluids were treated at 50 °C for 5 minutes, followed by 64 °C for 5 minutes with 100 mM TCEP and 1 mM EDTA. Error bars indicate 1 S.D. based on 3 technical replicates.

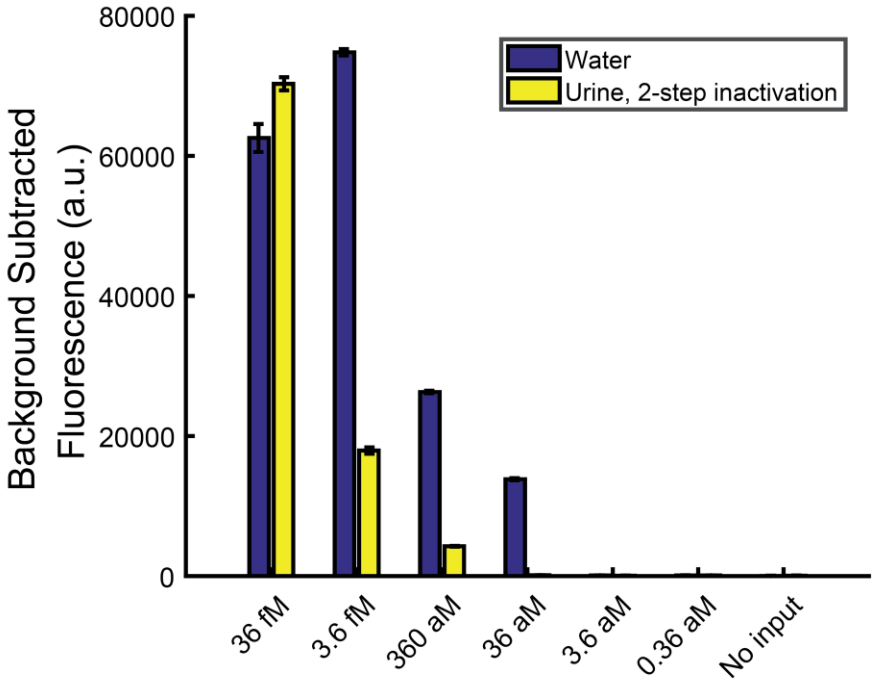

Fig. S13. RNase inactivation at a lower temperature.
We tested a two-step heat inactivation protocol in which healthy human urine was incubated at 50 °C for 20 minutes, followed by 95 °C for 5 minutes with 100 mM TCEP and 1 mM EDTA. RNA was diluted in urine after the 50 °C step but before the 95 °C step. Error bars indicate 1 S.D. based on 3 technical replicates.

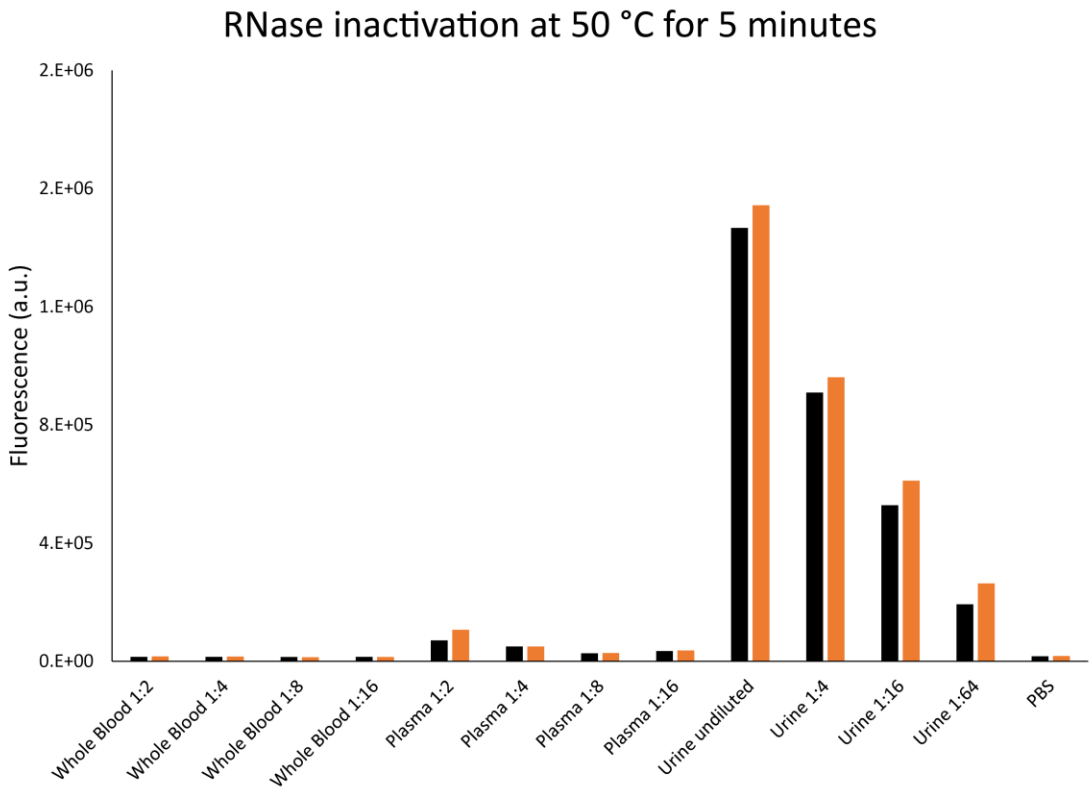

Fig. S14. Rapid RNase inactivation of whole blood, plasma, and urine.
Healthy human whole blood, plasma, and urine were diluted as indicated and inactivated at 50 °C for 5 minutes with 100 mM TCEP and 1 mM EDTA. RNase activity was measured using RNase Alert v2 (Thermo) in the presence of 2 U/µl Murine RNase inhibitor (NEB) after 1 hour of incubation at 37 °C. Two technical replicates are shown for each condition (orange and black bars).

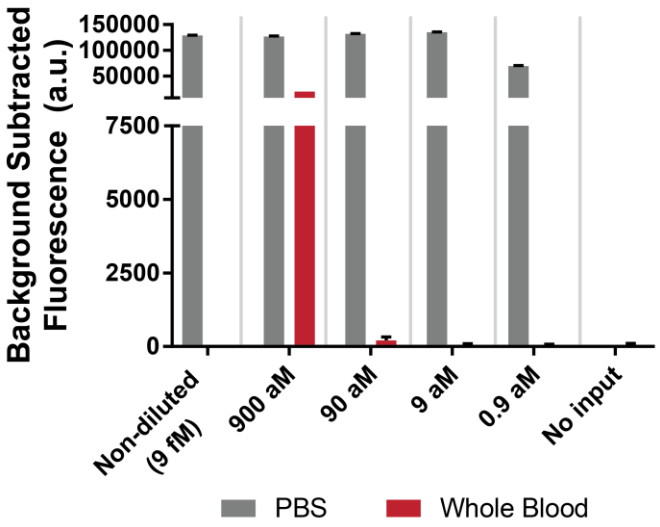

Fig. S15. Detection of Zika virus diluted in whole blood.
Detection of ZIKV RNA in particles diluted in healthy human whole blood (red) after 1 hour of detection. Samples were heated for 5 minutes at 50˚C plus 5 minutes at 64˚C with 100 mM TCEP and 1 mM EDTA. The same PBS control was used in Fig. 2A and Fig. 2B as the experiments were performed together. Error bars indicate 1 S.D. based on 3 technical replicates.

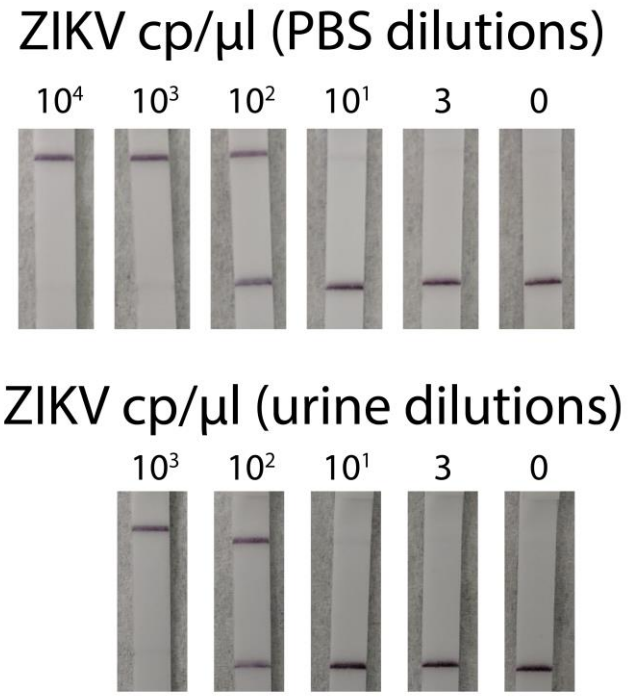

Fig. S16. Detection of Zika virus diluted in urine with a visual readout.
We show lateral flow detection of ZIKV diluted in urine (Fig. 2C). The top band is the test band and the bottom band is the control band. A faint band is visible at 10 copies per microliter in both PBS and urine dilutions after 1 hour of detection.

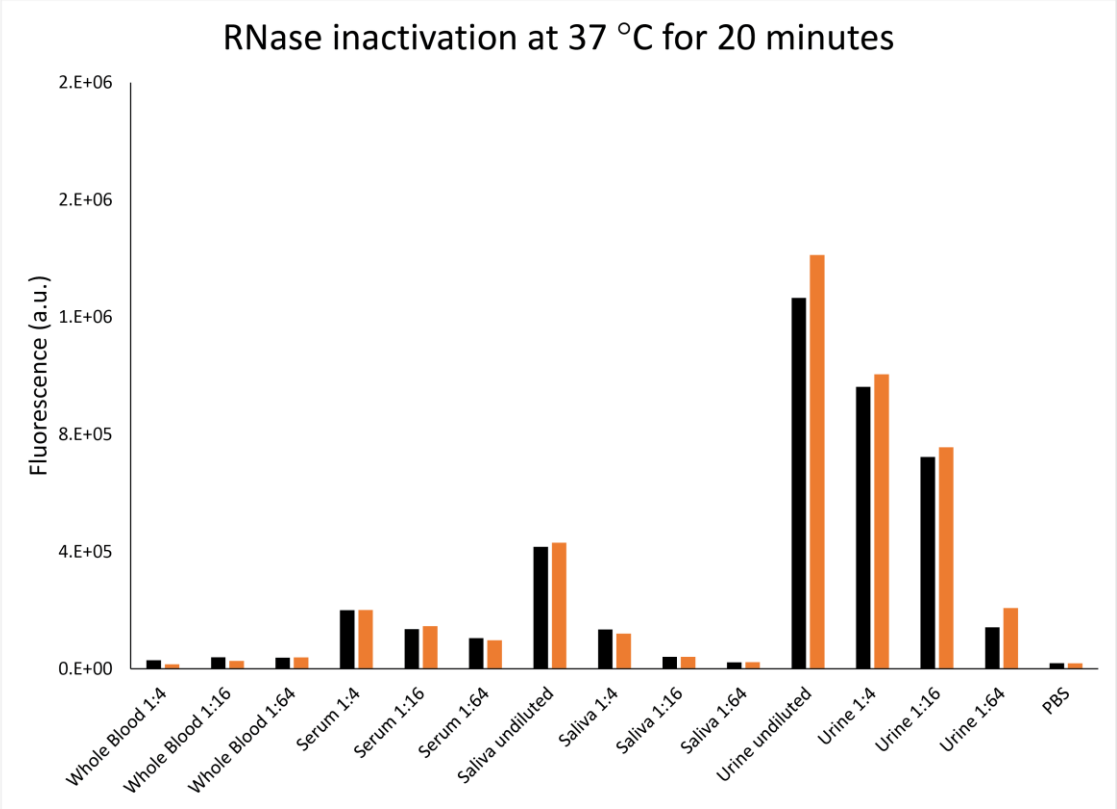

Fig. S17. Body-temperature heat inactivation of bodily fluids.
Healthy human whole blood, serum, saliva, and urine were diluted as indicated and inactivated at 37 °C for 20 minutes with 100 mM TCEP and 1 mM EDTA. RNase activity was measured using RNase Alert v2 (Thermo) in the presence of 2 U/µl Murine RNase inhibitor (NEB) after 1 hour of incubation at 37 °C. Two technical replicates are shown for each condition (orange and black bars).

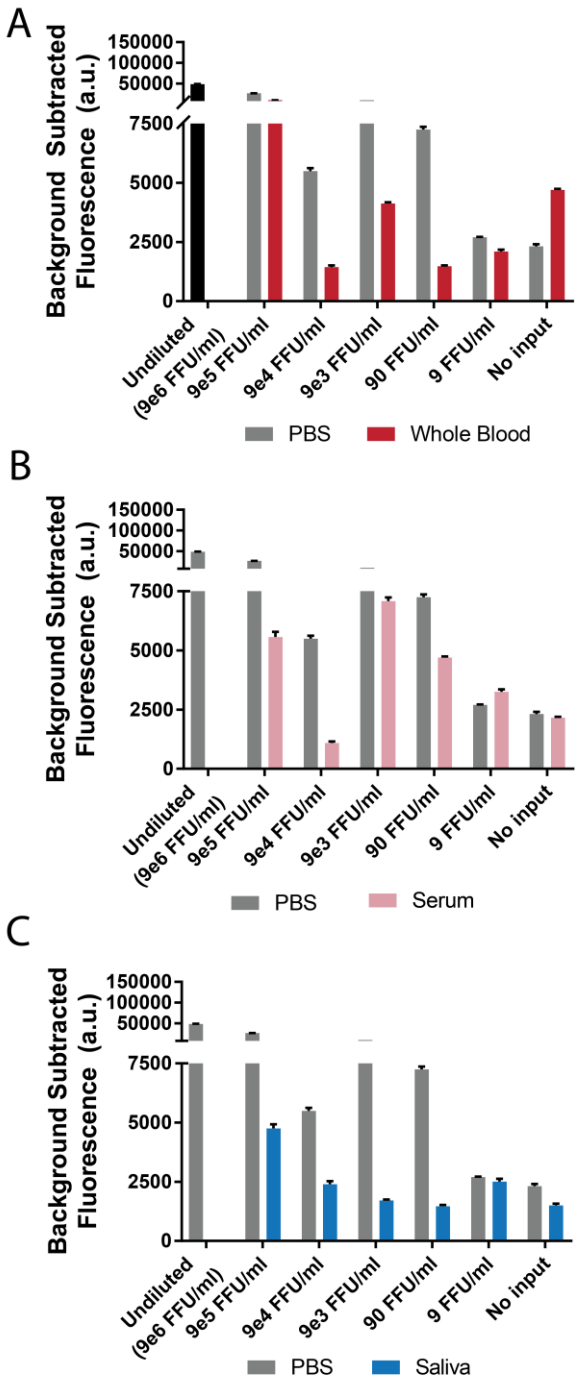

Fig. S18. Detection of dengue virus diluted in whole blood, serum, and saliva. Detection of DENV RNA in particles diluted in healthy human whole blood (red, A), serum (pink, B), or healthy human saliva (blue, C) after 1 hour of detection. Samples were heated for 20 minutes at 37 ˚C plus 5 minutes at 64˚C for inactivation with 100 mM TCEP and 1 mM EDTA. The same PBS controls used in all panels as the experiments were performed together. DENV titers in focus-forming units per ml (FFU/ml) are indicated. Error bars indicate 1 S.D. based on 3 technical replicates.

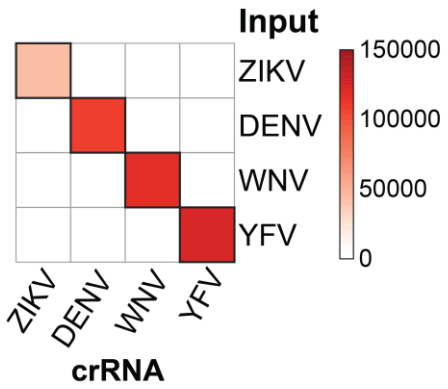

Fig. S19. Flavivirus panel heatmap.
Mean target-specific fluorescence for 3 technical replicates after 3 hours of Cas13 detection for each crRNA against each viral template. Targets were at 10^4 cp/µl. Rows: template input, columns: crRNAs tested. A bar plot of the same data is shown in Fig. 3B.

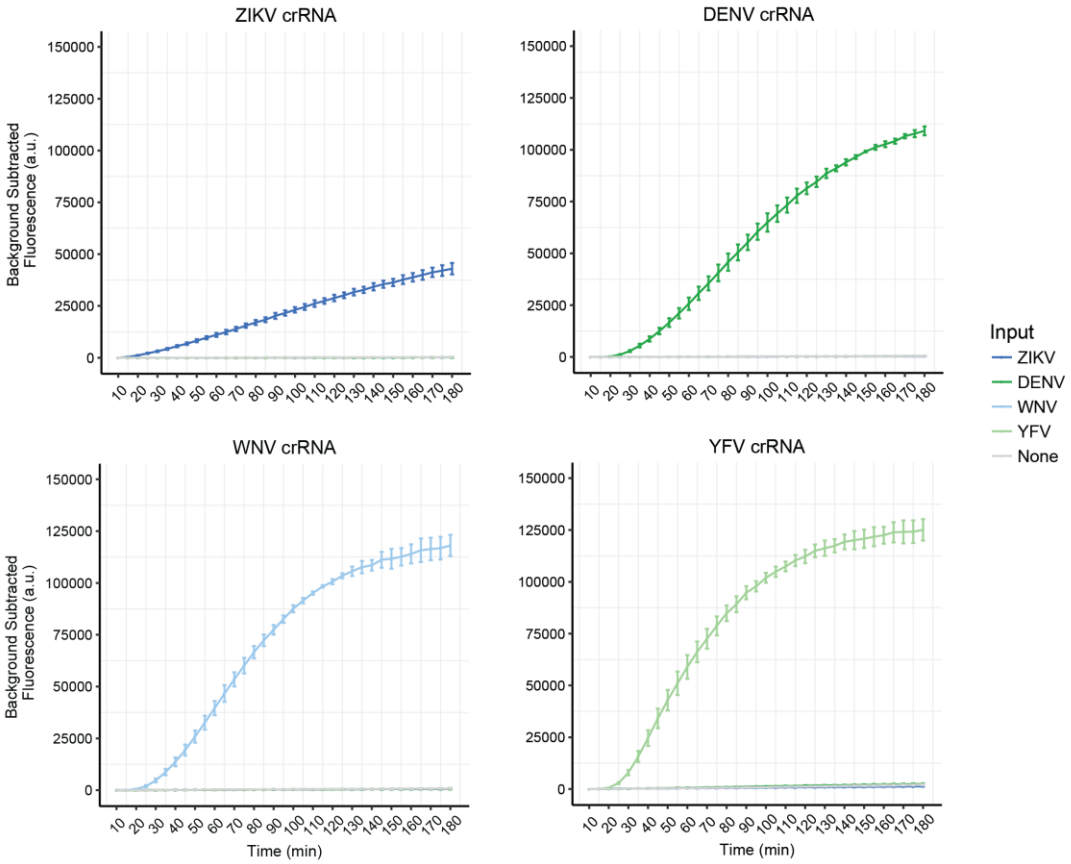

Fig. S20. Flavivirus panel time course.
Each panel shows the background-corrected fluorescence of a viral-specific crRNA against each flavivirus target and the no input control over a 3-hour time course with fluorescence measurements every 5 minutes. Targets were at 10^4 cp/µl and error bars are 1 S.D. based on 3 technical replicates.

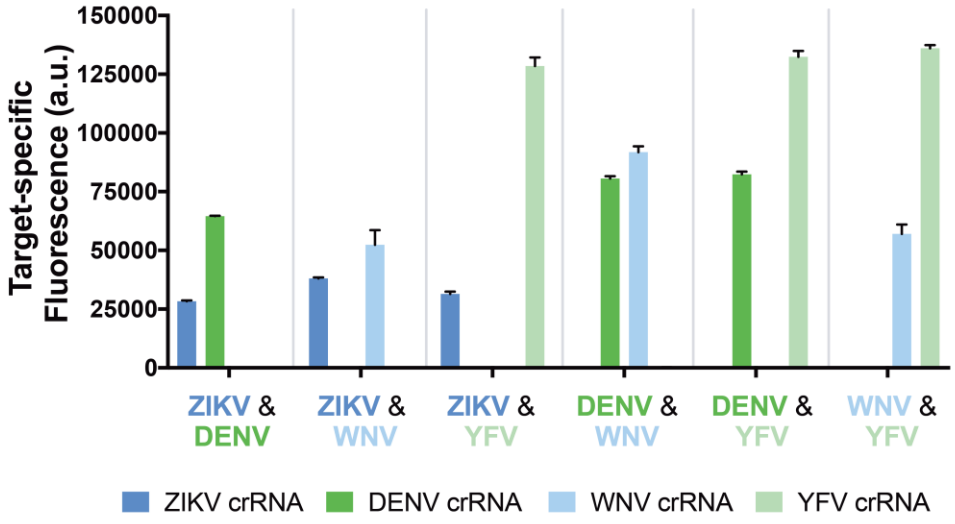

Fig. S21. Flavivirus panel co-infection bar chart.
Target-specific fluorescence after 3 hours of Cas13 detection is shown when two viral targets are present in a single sample. Target were at 10^4 cp/µl and error bars are at 1.S.D of 3 technical replicates. A heatmap of the same data is shown in Fig. 3C.

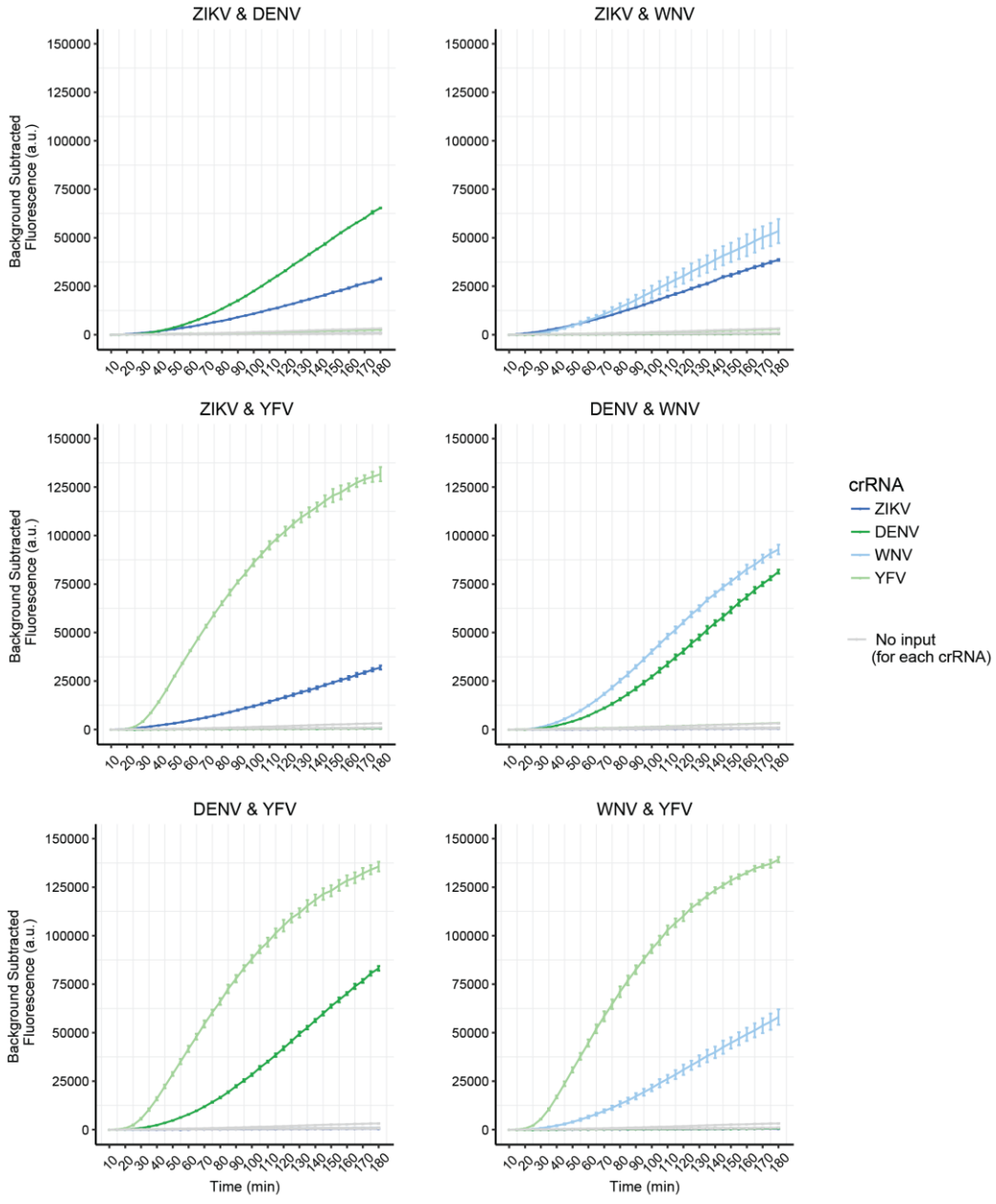

Fig. S22. Flavivirus panel co-infection time course.
Each panel shows the background-corrected fluorescence for all crRNAs against sample with two flavivirus targets over a 3-hour time course with fluorescence measurements every 5 minutes. Each panel also includes the background-corrected fluorescence observed for each crRNA against the no input control. Targets were at 10^4 cp/µl and error bars are 1 S.D. based on 3 technical replicates.

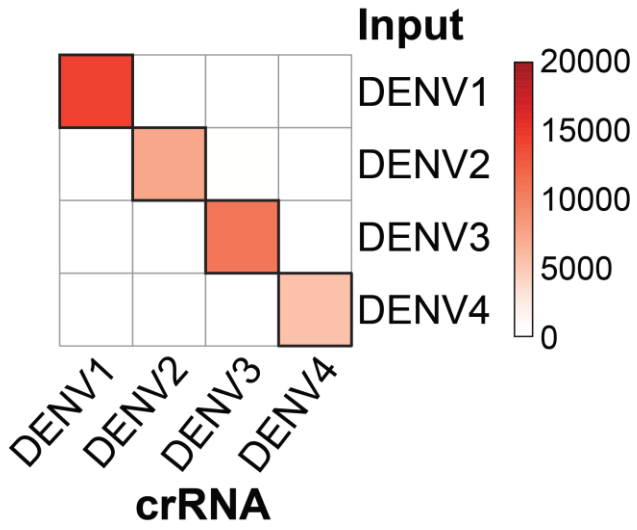

Fig. S23. Dengue synthetic template detection and heatmap
Mean target-specific fluorescence for 3 technical replicates after 3 hours of Cas13 detection for each crRNA against each viral template. Targets were at 10^4 cp/µl. Rows: template input, columns: crRNAs tested. A bar chart of this data is shown in Fig. 3E.

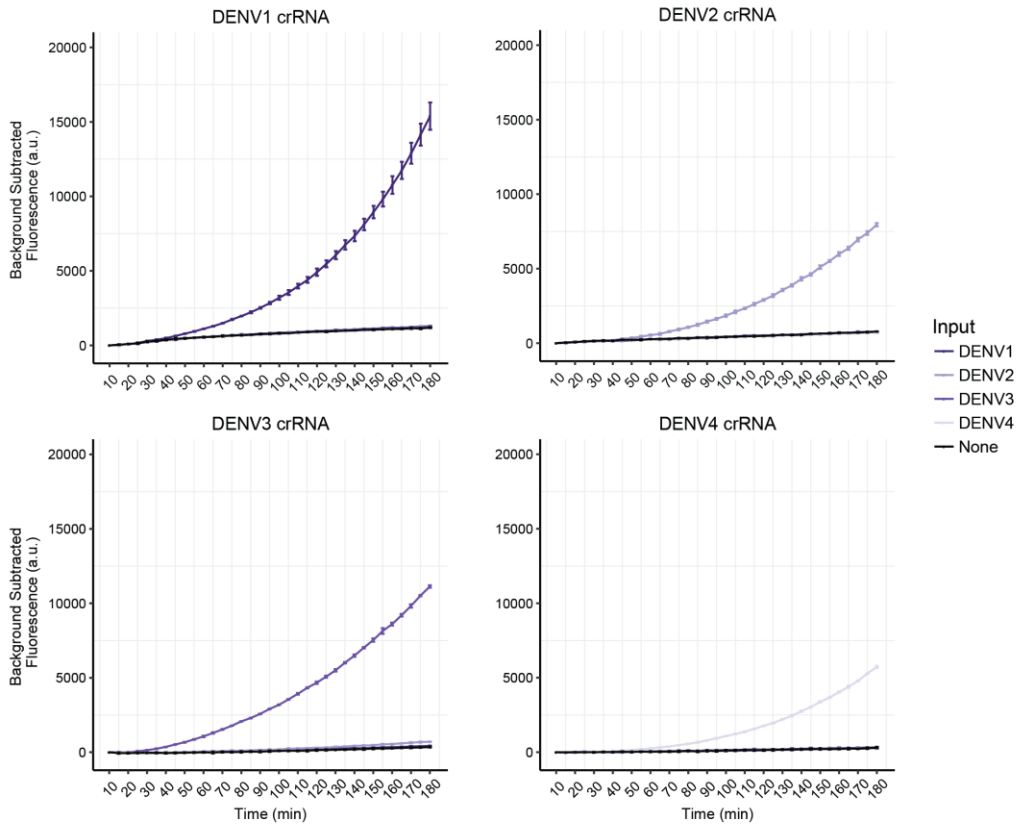

Fig. S24. Dengue panel time course.
Each panel shows the background-corrected fluorescence of a DENV serotype-specific crRNA against all DENV serotypes and a no input control over a 3-hour time course with fluorescence measurements every 5 minutes. Targets were at 10^4 cp/µl and error bars are 1 S.D. based on 3 technical replicates.

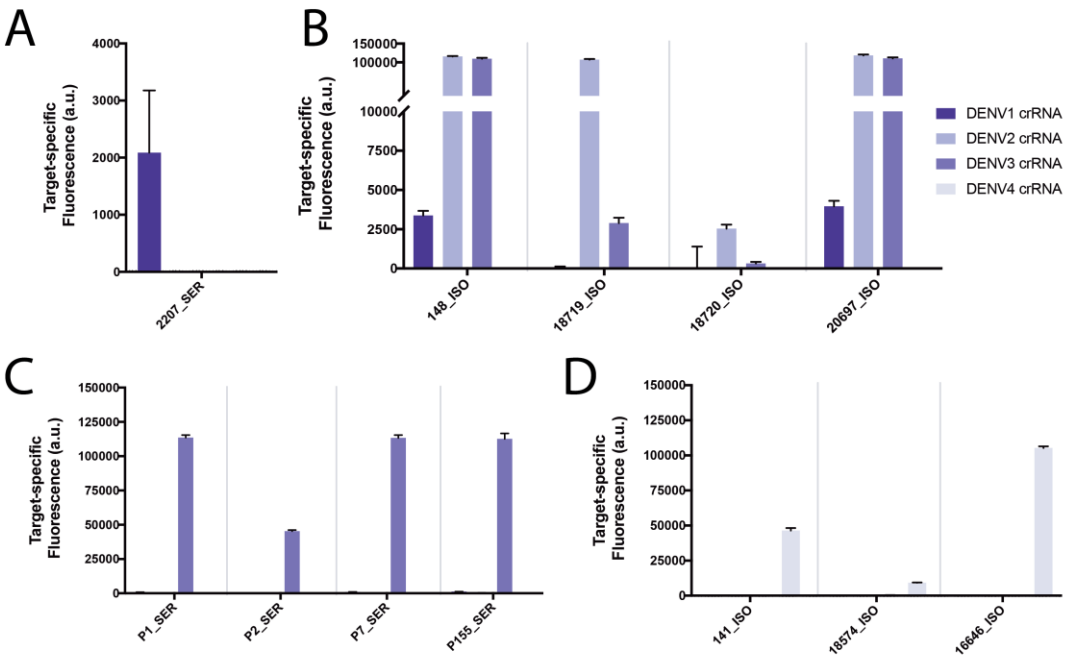

Fig. S25. Dengue clinical sample RNA serotype bar plots.
(A-D) SHERLOCK DENV panel for differentiating serotypes tested with extracted RNA from 1 DENV1 sample (A), 2 DENV2 samples and 2 samples with presence of DENV2 and DENV3 (B), 4 DENV3 samples (C), and 3 DENV4 samples (D). Fluorescence values are shown after 3 hours of Cas13 detection. Error bars indicate 1 S.D. based on 3 technical replicates.

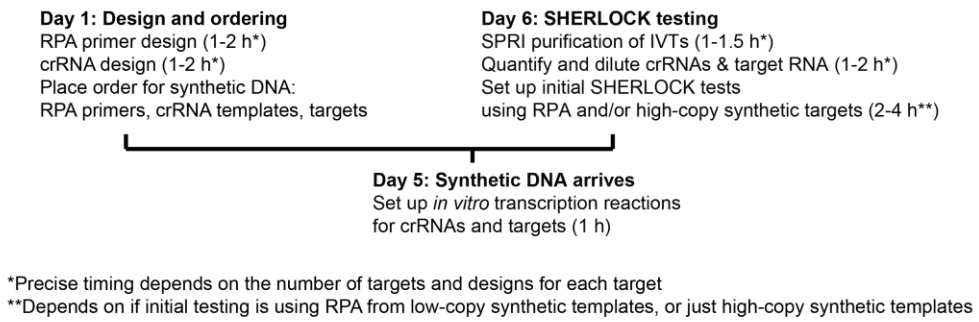

Fig. S26. SNP design timeline.
We show the steps required to design, build, and test a SHERLOCK-based SNP identification assay, along with the hands-on time required for each step. The total turnaround time is less than 1 week.

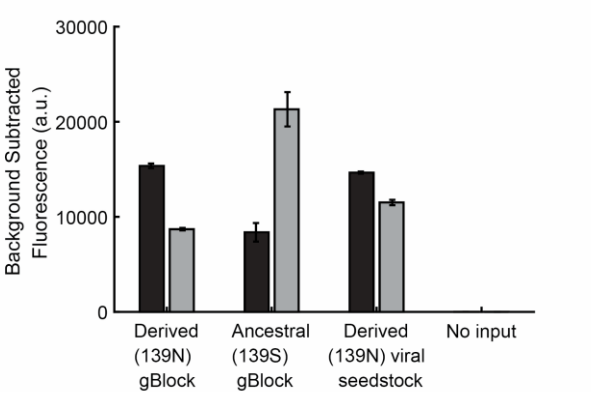

Fig. S27. Zika virus microcephaly-associated SNP discrimination with an alternative crRNA design.
The SNP is in the 7th position of the crRNA, and there is no synthetic mismatch introduced into the crRNA. Dark colors denote the derived crRNA and light colors denote the ancestral crRNA. This design was tested using synthetic targets (10^4 cp/μl) and viral seedstock cDNA ($3x10^2$ cp/μl) with 1 hour of Cas13 detection. Error bars indicate 1 S.D. based on 3 technical replicates.

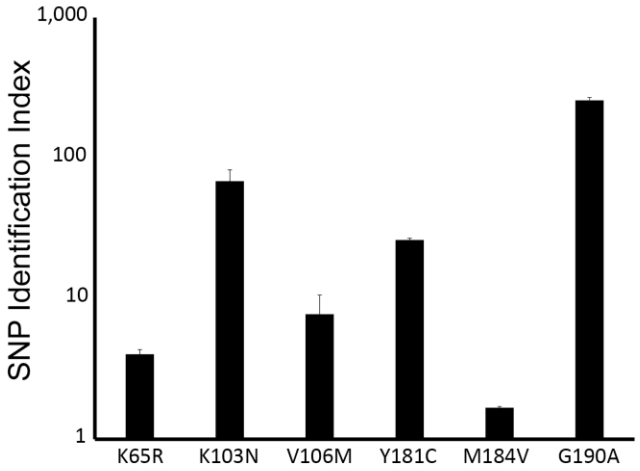

Fig. S28. SHERLOCK assays that can identify 6 drug-resistance mutations in HIV reverse transcriptase.
We show the SNP identification index, which is calculated by taking the fluorescence ratio for the derived template divided by the fluorescence ratio for the ancestral template (see Methods section for details). This index is equal to 1 if there is no ability to distinguish the ancestral and derived alleles, and increases with increasing ability to discriminate between the two alleles. Error bars indicate 1 S.D. based on 3 technical replicates.

Table S1. Metadata and nucleic acid testing for ZIKV clinical samples and mosquito pools.

We show a variety of information for the 40 ZIKV cDNA samples from the 2015-2016 ZIKV pandemic, including country of origin, sample type, and figure(s) used in. We also include the type and results of the ZIKV testing that were done at each of the collaborating sites. For the Aptima Zika Virus Assay signal over control (S/CO) values greater than 0 are considered positive and higher values denote more positive samples, although this assay is not quantitative. Faye-E and Lanciotti are published ZIKV primers and Ct values are listed when a RT-qPCR assay was performed. * See Table S2 for SHERLOCK results.

Sample	Country	Specimen type	Used in	Positive by SHERLOCK	Nucleic Acid Test Performed	Test result
DOM_2016_BB-0054-URI	Dominican Republic	Urine	Fig. 1, Fig. S2-S4	FALSE	Aptima Zika Virus Assay	30.77 (S/CO)
DOM_2016_BB-0054-SER	Dominican Republic	Serum	Fig. 1, Fig. S3	*	Aptima Zika Virus Assay	34.05 (S/CO)
DOM_2016_BB-0059-URI	Dominican Republic	Urine	Fig. 1, Fig. S2-S4	TRUE	Aptima Zika Virus Assay	33.67 (S/CO)
DOM_2016_BB-0059-SER	Dominican Republic	Serum	Fig. 1, Fig. S2-S4	FALSE	Aptima Zika Virus Assay	35.07 (S/CO)
DOM_2016_BB-0071-SER	Dominican Republic	Serum	Fig. 1, Fig. S2-S4	TRUE	Aptima Zika Virus Assay	34.57 (S/CO)
DOM_2016_BB-0071-URI	Dominican Republic	Urine	Fig. 1, Fig. S3	*	Aptima Zika Virus Assay	0 (S/CO)
DOM_2016_BB-0076-SER	Dominican Republic	Serum	Fig. 1, Fig. S2-S4	TRUE	Aptima Zika Virus Assay	33.45 (S/CO)
DOM_2016_BB-0076-URI	Dominican Republic	Urine	Fig. 1, Fig. S2-S4	TRUE	Aptima Zika Virus Assay	36.68 (S/CO)
DOM_2016_BB-0085-URI	Dominican Republic	Urine	Fig. 1, Fig. S2-S4	TRUE	Aptima Zika Virus Assay	0 (S/CO)
DOM_2016_BB-0085-SER	Dominican Republic	Serum	Fig. 1, Fig. S3	*	Aptima Zika Virus Assay	33.04 (S/CO)

DOM_2016_BB-0091-SER	Dominican Republic	Serum	Fig. 1, Fig. S2-S4	TRUE	Aptima Zika Virus Assay	31.8 (S/CO)
DOM_2016_BB-0115-SER	Dominican Republic	Serum	Fig. 1, Fig. 4, Fig. S2-S4	TRUE	Aptima Zika Virus Assay	27.78 (S/CO)
DOM_2016_BB-0115-URI	Dominican Republic	Urine	Fig. 1, Fig. S2, S4	TRUE	None	N/A
DOM_2016_BB-0127-SER	Dominican Republic	Serum	Fig. 1, Fig. S2-S4	TRUE	Aptima Zika Virus Assay	32.95 (S/CO)
DOM_2016_BB-0180-SER	Dominican Republic	Serum	Fig. 1, Fig. S2-S4	TRUE	Aptima Zika Virus Assay	31.93 (S/CO)
DOM_2016_BB-0180-URI	Dominican Republic	Urine	Fig. 1, Fig. S2-S4	FALSE	Aptima Zika Virus Assay	36.8 (S/CO)
DOM_2016_BB-0183-SER	Dominican Republic	Serum	Fig. 1, Fig. S2-S4	TRUE	Aptima Zika Virus Assay	33.64 (S/CO)
DOM_2016_BB-0183-URI	Dominican Republic	Urine	Fig. 1, Fig. S2-S4	FALSE	Aptima Zika Virus Assay	0 (S/CO)
DOM_2016_BB-0184-URI	Dominican Republic	Urine	Fig. 1, Fig. S2, S4	TRUE	None	N/A
USA_2016_FL-01-MOS	United States	Mosquito Pool	Fig. S2-S4	TRUE	Faye-E (Faye, O. 2008), gel electrophoresis	+
USA_2016_FL-02-MOS	United States	Mosquito Pool	Fig. 4, Fig. S2-S4	TRUE	Faye-E (Faye, O. 2008), gel electrophoresis	+
USA_2016_FL-03-MOS	United States	Mosquito Pool	Fig. S2-S4	TRUE	Faye-E (Faye, O. 2008), gel electrophoresis	+
USA_2016_FL-021-URI	United States	Urine	Fig. 1, Fig. S2, S4	TRUE	Faye-E (Faye, O. 2008)	Ct 27.57
USA_2016_FL-029-URI	United States	Urine	Fig. 1, Fig. S2, S4	FALSE	Faye-E (Faye, O. 2008)	Ct 33.6
USA_2016_FL-030-URI	United States	Urine	Fig. 1, Fig. S2, S4	TRUE	Faye-E (Faye, O. 2008)	Ct 29.27

HND_2016_HU-ME33-PLA	Honduras	Plasma	Fig. 1, Fig. S2, S4	FALSE	Lanciotti (Lanciotti, R.S. 2008)	Ct 33.35
HND_2016_HU-ME38-PLA	Honduras	Plasma	Fig. 1, Fig. S2, S4	TRUE	Lanciotti (Lanciotti, R.S. 2008)	Ct 29.95
HND_2016_HU-ME42-SER	Honduras	Serum	Fig. 1, Fig. S2, S4	TRUE	Lanciotti (Lanciotti, R.S. 2008)	Ct 33.45
HND_2016_HU-ME50-PLA	Honduras	Plasma	Fig. 1, Fig. S2, S4	FALSE	Lanciotti (Lanciotti, R.S. 2008)	Ct 33.45
HND_2016_HU-ME58-PLA	Honduras	Plasma	Fig. 1, Fig. 4, Fig. S2, S4	TRUE	Lanciotti (Lanciotti, R.S. 2008)	Ct 33.55
HND-2016_HU-ME59-PLA	Honduras	Plasma	Fig. 1, Fig. S2, S4	TRUE	Lanciotti (Lanciotti, R.S. 2008)	Ct 33.6
HND_2016_HU-ME131-PLA	Honduras	Plasma	Fig. 1, Fig. S2, S4	TRUE	Lanciotti (Lanciotti, R.S. 2008)	Ct 34.15
HND_2016_HU-ME136-PLA	Honduras	Plasma	Fig. 1, Fig. S2, S4	FALSE	Lanciotti (Lanciotti, R.S. 2008)	Ct 35.1
HND_2016_HU-ME137-PLA	Honduras	Plasma	Fig. 1, Fig. S2-S4	FALSE	Lanciotti (Lanciotti, R.S. 2008)	Ct 35.3
HND-2016_HU-ME147-SER	Honduras	Serum	Fig. 1, Fig. S2, S4	TRUE	Lanciotti (Lanciotti, R.S. 2008)	Ct 34.15
HND_2016_HU-ME152-SER	Honduras	Serum	Fig. 1, Fig. S2, S4	TRUE	Lanciotti (Lanciotti, R.S. 2008)	Ct 33.9
HND_2016_HU-ME156-SER	Honduras	Serum	Fig. 1, Fig. S2, S4	TRUE	Lanciotti (Lanciotti, R.S. 2008)	Ct 34.15
HND_2016_HU-ME167-PLA	Honduras	Plasma	Fig. 1, Fig. S2, S4	TRUE	Lanciotti (Lanciotti, R.S. 2008)	Ct 32.9
HND-2016_HU-ME171-PLA	Honduras	Plasma	Fig. 1, Fig. S2, S4	TRUE	Lanciotti (Lanciotti, R.S. 2008)	Ct 34.85

HND_2016_HU-ME172-PLA	Honduras	Plasma	Fig. 1, Fig. S2, S4	FALSE	Lanciotti (Lanciotti, R.S. 2008)	Ct 34.25
HND_2016_HU-ME178-PLA	Honduras	Plasma	Fig. 1, Fig. S2, S4	TRUE	Lanciotti (Lanciotti, R.S. 2008)	Ct 34.35
HND_2016_HU-ME180-PLA	Honduras	Plasma	Fig. 1, Fig. S2, S4	FALSE	Lanciotti (Lanciotti, R.S. 2008)	Ct 33.25
HND_2016_HU-SZ76-SER	Honduras	Serum	Fig. 1, Fig. S2, S4	FALSE	Lanciotti (Lanciotti, R.S. 2008)	Ct 25.55

Table S2. Results of SHERLOCK compared to Hologic and Altona ZIKV nucleic acid tests.

SHERLOCK fluorescence mean and S.D. are based on 3 technical replicates. For the Hologic assay, samples are positive when signal/cutoff is greater than 0. For the Altona assay, samples are positive when Ct values are less than 36 as defined by the kit specifications.

Sample	Country	Specimen type	SHERLOCK fluorescence @ 3 h (mean)	SHERLOCK fluorescence @ 3 h (SD)	Positive by Hologic	Positive by Altona
DOM_2016_BB-0054-URI	Dominican Republic	Urine	40.3333333	23.11565126	TRUE	FALSE
DOM_2016_BB-0054-SER	Dominican Republic	Serum	91.6666667	65.49300217	TRUE	FALSE
DOM_2016_BB-0059-URI	Dominican Republic	Urine	114	70.4485628	TRUE	FALSE
DOM_2016_BB-0059-SER	Dominican Republic	Serum	57987.6667	1704.081082	TRUE	TRUE
DOM_2016_BB-0071-SER	Dominican Republic	Serum	114336	1429.226364	TRUE	TRUE
DOM_2016_BB-0071-URI	Dominican Republic	Urine	58	46.13025038	TRUE	FALSE
DOM_2016_BB-0076-URI	Dominican Republic	Urine	75539.3333	961.4345185	TRUE	TRUE
DOM_2016_BB-0085-URI	Dominican Republic	Urine	29.3333333	43.01550108	FALSE	FALSE
DOM_2016_BB-0085-SER	Dominican Republic	Serum	123215.333	14872.59511	TRUE	TRUE
DOM_2016_BB-0091-SER	Dominican Republic	Serum	112993	2131.246349	TRUE	TRUE
DOM_2016_BB-0115-SER	Dominican Republic	Serum	97830.6667	2968.648233	TRUE	TRUE
DOM_2016_BB-0127-SER	Dominican Republic	Serum	80429.3333	6778.087218	TRUE	TRUE
DOM_2016_BB-0180-SER	Dominican Republic	Serum	85652.6667	4965.606341	TRUE	TRUE

DOM_2016_BB-0180-URI	Dominican Republic	Urine	578.333333	9.504384953	TRUE	TRUE
DOM_2016_BB-0183-SER	Dominican Republic	Serum	112883.667	1027.309755	TRUE	TRUE
DOM_2016_BB-0183-URI	Dominican Republic	Urine	61.6666667	43.54690957	FALSE	FALSE

Table S3. SHERLOCK and amplicon PCR results for ZIKV clinical samples and mosquito pools.

We show a variety of information for the 40 ZIKV cDNA samples from the 2015-2016 ZIKV pandemic, including country of origin, sample type. We include the SHERLOCK fluorescence (mean and standard deviation) after 1 hour, as well as the amplicon PCR pool 1 and pool 2 concentrations, and the amplicon PCR yield (defined as the minimum of the two primer pool concentrations.

Sample	Country	Specimen type	SHERLOCK fluorescence @ 1h (mean)	SHERLOCK fluorescence @ 1 h (SD)	Amplicon PCR pool 1 conc. (ng/ul)	Amplicon PCR pool 2 conc. (ng/ul)	Amplicon PCR yield (ng/ul)
DOM_2016_BB-0054-URI	Dominican Republic	Urine	64	28.35489	0	0.3	0
DOM_2016_BB-0059-URI	Dominican Republic	Urine	4042.333	124.5084	0.2	0.5	0.2
DOM_2016_BB-0059-SER	Dominican Republic	Serum	88	104.6518	2.7	3.4	2.7
DOM_2016_BB-0071-SER	Dominican Republic	Serum	456	103.0146	4.5	3.4	3.4
DOM_2016_BB-0076-SER	Dominican Republic	Serum	311.6667	38.00439	2.9	2.7	2.7
DOM_2016_BB-0076-URI	Dominican Republic	Urine	3114	570.8704	1.7	0	0
DOM_2016_BB-0085-URI	Dominican Republic	Urine	473.6667	50.80682	8.1	12.3	8.1
DOM_2016_BB-0091-SER	Dominican Republic	Serum	30426.67	7086.829	17.5	19	17.5
DOM_2016_BB-0115-SER	Dominican Republic	Serum	77020	16146.71	16.4	41.8	16.4
DOM_2016_BB-0115-URI	Dominican Republic	Urine	8701.667	2008.831	4.7	8	4.7

DOM_2016_BB-0127-SER	Dominican Republic	Serum	87383	923.0596	65.6	80	65.6
DOM_2016_BB-0180-SER	Dominican Republic	Serum	80265	156.9044	6.4	8.2	6.4
DOM_2016_BB-0180-URI	Dominican Republic	Urine	41.33333	49.09515	4.5	8.1	4.5
DOM_2016_BB-0183-SER	Dominican Republic	Serum	8689	912.5004	11.9	15.7	11.9
DOM_2016_BB-0183-URI	Dominican Republic	Urine	62.66667	52.65295	0	0.1	0
DOM_2016_BB-0184-URI	Dominican Republic	Urine	3065.667	157.8618	0.3	0	0
USA_2016_FL-01-MOS	United States	Mosquito Pool	35490	513.0731	58.9	144	58.9
USA_2016_FL-02-MOS	United States	Mosquito Pool	10314	115.1043	67.7	76.9	67.7
USA_2016_FL-03-MOS	United States	Mosquito Pool	60385.67	791.5013	69.8	87.5	69.8
USA_2016_FL-021-URI	United States	Urine	16201	283.1042	8	10.2	8
USA_2016_FL-029-URI	United States	Urine	119	48.6621	0.7	1.29	0.7
USA_2016_FL-030-URI	United States	Urine	235.6667	53.52881	7.2	10.1	7.2
HND_2016_HU-ME33-PLA	Honduras	Plasma	45	57.8619	2.7	1	1
HND_2016_HU-ME38-PLA	Honduras	Plasma	33957.33	687.6717	61.9	66.8	61.9
HND_2016_HU-ME42-SER	Honduras	Serum	20041.67	189.9746	28.3	38.6	28.3

HND_2016_HU-ME50-PLA	Honduras	Plasma	106.6667	23.15887	2.4	4.8	2.4
HND_2016_HU-ME58-PLA	Honduras	Plasma	12284	303.287	36.3	38.6	36.3
HND-2016_HU-ME59-PLA	Honduras	Plasma	7115	167.9196	14.2	17	14.2
HND_2016_HU-ME131-PLA	Honduras	Plasma	8452.333	97.72581	8.7	13.4	8.7
HND_2016_HU-ME136-PLA	Honduras	Plasma	35	47.69696	1.1	3.3	1.1
HND_2016_HU-ME137-PLA	Honduras	Plasma	23.66667	23.43786	1	1.1	1
HND-2016_HU-ME147-SER	Honduras	Serum	4625.667	41.501	8.6	12.4	8.6
HND_2016_HU-ME152-SER	Honduras	Serum	2165	50.47772	14.7	20.7	14.7
HND_2016_HU-ME156-SER	Honduras	Serum	853.3333	163.0164	8.1	6.2	6.2
HND_2016_HU-ME167-PLA	Honduras	Plasma	15552.67	2654.519	16.7	34.1	16.7
HND-2016_HU-ME171-PLA	Honduras	Plasma	4832.667	832.8771	4.1	6.1	4.1
HND_2016_HU-ME172-PLA	Honduras	Plasma	171.3333	46.73685	1.9	2.9	1.9
HND_2016_HU-ME178-PLA	Honduras	Plasma	1108	47.0319	18.8	24.4	18.8
HND_2016_HU-ME180-PLA	Honduras	Plasma	82.66667	49.81298	6.2	4.9	4.9
HND_2016_HU-SZ76-SER	Honduras	Serum	110.3333	45.6545	0.8	0.5	0.5

Table S4. Metadata for DENV patient samples and clinical isolates.

We show a variety of information for the 24 DENV RNA samples, 8 serum patient samples 3 saliva samples including country of origin, sample type, and figure(s) used in.

Sample	Country	Specimen type	Used in
2207_SER	Colombia	RNA (serum)	Fig. 1, Fig. 3, Fig. S7, S25
3736_SER	Colombia	RNA (serum)	Fig. 1, Fig. S7
3739_SER	Colombia	RNA (serum)	Fig. 1, Fig. S7
3742_SER	Colombia	RNA (serum)	Fig. 1, Fig. S7
3745_SER	Colombia	RNA (serum)	Fig. 1, Fig. S7
3754_SER	Colombia	RNA (serum)	Fig. 1, Fig. S7
3764_SER	Colombia	RNA (serum)	Fig. 1, Fig. S7
3766_SER	Colombia	RNA (serum)	Fig. 1, Fig. S7
2280_SER	Colombia	RNA (serum)	Fig. 1, Fig. S7
148_ISO	Colombia	RNA (clinical isolate)	Fig. 1, Fig. 3, Fig. S7, Fig. S25
141_ISO	Colombia	RNA (clinical isolate)	Fig. 1, Fig. 3, Fig. S7, Fig. S25
142_ISO	Colombia	RNA (clinical isolate)	Fig. 1, Fig. S7
16646_ISO	Mexico	RNA (clinical isolate)	Fig. 1, Fig. 3, Fig. S7, Fig. S25
18565_ISO	Mexico	RNA (clinical isolate)	Fig. 1, Fig. S7
18574_ISO	Mexico	RNA (clinical isolate)	Fig. 1, Fig. 3, Fig. S7, Fig. S25

18719_ISO	Mexico	RNA (clinical isolate)	Fig. 1, Fig. 3, Fig. S7, Fig. S25
18720_ISO	Mexico	RNA (clinical isolate)	Fig. 1, Fig. 3, Fig. S7, Fig. S25
20693_ISO	Mexico	RNA (clinical isolate)	Fig. 1, Fig. S7
20697_ISO	Mexico	RNA (clinical isolate)	Fig. 1, Fig. 3, Fig. S7, Fig. S25
P1_SER	Peru	RNA (serum)	Fig. 1, Fig. 3, Fig. S7, Fig. S25
P2_SER	Peru	RNA (serum)	Fig. 1, Fig. 3, Fig. S7, Fig. S25
P7_SER	Peru	RNA (serum)	Fig. 1, Fig. 3, Fig. S7, Fig. S25
P155_SER	Peru	RNA (serum)	Fig. 1, Fig. 3, Fig. S7, Fig. S25
P164_SER	Peru	RNA (serum)	Fig. 1, Fig. S7
BB_20544 _SER	Peru	Serum	Fig. 2
BB_20545_SER	Peru	Serum	Fig. 2
BB_20547_ SER	Peru	Serum	Fig. 2
BB_20553_SER	Peru	Serum	Fig. 2
BB_20545_SAL	Peru	Saliva	Fig. 2
BB_20547_SAL	Peru	Saliva	Fig. 2
BB_20553_ SAL	Peru	Saliva	Fig. 2
RPDen06/74	Brazil	Serum	Fig. 2
VDen06/27	Brazil	Serum	Fig. 2

RPDen06/31	Brazil	Serum	Fig. 2
RPDen08/293	Brazil	Serum	Fig. 2

Table S5. List of RPA primer sequences used in this study.

Forward primers contain the T7 promoter sequence primer (gaaatTAATACGACTCACTATAggg) at their 5' end.

RPA Primer Name	Used in	Sequence	Reference
RP819	Fig. 1, Fig. 2, Fig. S1-S3, Fig. S9-S12, Fig. S15, Fig. S16	gaaatTAATACGACTCACTATAGGGCGTGGCGCACTACATGTACT	Gootenberg *et al.* 2017
RP821	Fig. 1, Fig. 2, Fig. S1-S3, Fig. S9-S12, Fig. S15, Fig. S16	TGTCAATGTCAGTCACCACTATTCCATCCA	Gootenberg *et al.* 2017
DENV1-3-RPA-RP4	Fig. 1, Fig. 2, Fig. S6, Fig. S7, Fig. S18	gaaatTAATACGACTCACTATAggAACAGCATATTGACGCTGGGAGAGACCAGAGATC	Abd El Wahed, A. *et. al.* 2015
DENV1-3-RPA-FP13	Fig. 1, Fig. 2, Fig. S6, Fig. S7, Fig. S18	ATTCAACAGCACCATTCCATTTTCTGGCGTTCTGTG	Abd El Wahed, A. *et. al.* 2015
DENV4-RPA-RP2	Fig. 1, Fig. 2, Fig. S6, Fig. S7, Fig. S18	gaaatTAATACGACTCACTATAggCACAAAAACAGCATATTGACGCTGGGAAAG	Abd El Wahed, A. *et. al.* 2015
DENV4-RPA-FP3	Fig. 1, Fig. 2, Fig. S6, Fig. S7, Fig. S18	CATCTTGCGGCGCTCTGTGCCTGGATTGA	Abd El Wahed, A. *et. al.* 2015
FLAVI-NS5fwd-1	Fig. 3, Fig. S19-S22	gaaatTAATACGACTCACTATAGGGGTACAACATGATGGGGAARAGAGARAARAA	This study
FLAVI-NS5rev-1	Fig. 3, Fig. S19-S22	CGKGTGTCCCAGCCNGCKGTGTCATCWGCA	This study
DENV-3UTRfwd-1	Fig. 3, Fig. S23-25	gaaatTAATACGACTCACTATAGGGTTGAGCAAACCGTGCTGCCTGTAGCTCC	This study
DENV-3UTRrev-1	Fig. 3, Fig. S23-25	GGGAGGGGTCTCCTCTAACCRCTAGTC	This study
DOMUSA-5249-	Fig. 4	gaaatTAATACGACTCACTATAG	This study

fwd		GGACTGTCTTAGACTTGCATCCTGGAGCTGGG	
DOMUSA-5249-rev	Fig. 4	CTTCCTCCATTTCAGCAGCGACAACCCTGG	This study
USA-935-fwd	Fig. 4	gaaatTAATACGACTCACTATAGGGTAGAGTCGAAAATTGGATATTCAGGAACCC	This study
USA-935-rev	Fig. 4	AACCCAAGTCCCACCTGACATACCTTCCAC	This study
HND-2788-fwd	Fig. 4	gaaatTAATACGACTCACTATAGGGTGGAAGAGAATGGAGTTCAACTGACGGTCG	This study
HND-2788-rev	Fig. 4	GAAGTGCGATTTCCCCCAAGCCTTCCAGCC	This study
ZIKV-mcep-fwd	Fig. 4, Fig. S27	gaaatTAATACGACTCACTATAGGGTACTAGTGTCGGAATTGTTG	This study
ZIKV-mcep-rev	Fig. 4, Fig. S27	TAACACTTATTCATCCCCAATGTGGTTG	This study
HIVRT-149F	Fig. S28	gaaatTAATACGACTCACTATAggggTTGGGCCTGAAAATCCATACAATACTCCAG	This study
HIVRT-348R	Fig. S28	AAAATATGCATCACCCACATCCAGTACTG	This study
HIVRT-462F	Fig. S28	gaaatTAATACGACTCACTATAggggAGGATCACCAGCAATATTCCAAAGTAGCATG	This study
HIVRT-601R	Fig. S28	TTGTTCTATGCTGCCCTATTTCTAAGTCAG	This study

Table S6. List of crRNA spacer sequences used in this study.

All crRNAs used in this study contain the same direct repeat sequence (GAUUUAGACUACCCCAAAAACGAAGGGGACUAAAAC). A 5' GGG for increased yield during T7 *in vitro* transcription is encoded in the T7 promoter sequence primer (gaaatTAATACGACTCACTATAggg).

crRNA Name	Used in	Spacer Sequence	Reference
Zika targeting crRNA 2	Fig. 1, Fig. 2, Fig. S1-S3, Fig. S9-S12, Fig. S15, Fig. S16	UGCUGCCUGCAGCCCUGGGAUCAAGUAC	Gootenberg *et al.* 2017
D1-3UTRat10660	Fig. 1, Fig. 2, Fig. S6, Fig. S7, Fig. S18	UGGAAUGAUGCUGUAGAGACAGCAGGAU	This study
D2/3-3UTRat10635	Fig. 1, Fig. 2, Fig. S6, Fig. S7, Fig. S18	GAGGAGACAGCAGGAUCUCUGGUCUUUC	This study
D4-3UTRat10620	Fig. 1, Fig. 2, Fig. S6, Fig. S7, Fig. S18	UGGAUUGAUGUUGCAGAGACAGCAGGAU	This study
ZIKV-NS5at9227	Fig. 3, Fig. S19-S22	UCCUCCUGGUAUGCGACUCAUCUCUUCU	This study
DENV-NS5at9127	Fig. 3, Fig. S19-S22	UCCCCCUGGAAUCUUUGAUAUGUCUCUG	This study
WNV-NS5at9243	Fig. 3, Fig. S19-S22	GCCCCCAGGCCGGGUGCCAACUUCACGC	This study
YFV-NS5at9122	Fig. 3, Fig. S19-S22	AUUCUCUCUGGAUGCCCAGUGGUCUUCA	This study
D1-3UTRat10457	Fig. 3, Fig. S23-25	AUGGGUUGCAGCCUCCCGGGUUUUUACA	This study
D2-3UTRat10433	Fig. 3, Fig. S23-25	GGCCUCCCAGAUUUUUUACACCUUCUCA	This study
D3-3UTRat10419	Fig. 3, Fig. S23-25	CACGGUUUGCAGCCUCCCAGGCUUUACG	This study
D4-3UTRat10366	Fig. 3, Fig. S23-25	UGGCGCAUGGCCUCCCUGGGAAUUUUAC	This study
DOMUSA-5249-ancestral	Fig. 4	auggguucacggacuauuucaggaagaa	This study

DOMUSA-5249-derived	Fig. 4	auagguucacggacuauuucaggaagaa	This study
USA-935-ancestral	Fig. 4	augaguuuuuggcucguugagcuuccca	This study
USA-935-derived	Fig. 4	auaaguuuuuggcucguugagcuuccca	This study
HND-2788-ancestral	Fig. 4	gaccacuccacauggggguuuuuacaga	This study
HND-2788-derived	Fig. 4	gagcacuccacauggggguuuuuacaga	This study
ZIKV-mcep-snp3syn5-derived	Fig. 4, Fig. S27	cguuacuguccaaguacauYuaguaugc	This study
ZIKV-mcep-snp3syn5-ancestral	Fig. 4, Fig. S27	cgcuacuguccaaguacauYuaguaugc	This study
ZIKV-mcep-snp7-ancestral	Fig. 4, Fig. S27	gcaucguuucuguccaaguacauYuagu	This study
ZIKV-mcep-snp7-derived	Fig. 4, Fig. S27	gcaucgcuucuguccaaguacauYuagu	This study
HIVRT-K65R-ancestral	Fig. S28	UUUUGUUUAUGGCAAAUACUGGAGUAUU	This study
HIVRT-K65R-derived	Fig. S28	UUCUGUUUAUGGCAAAUACUGGAGUAUU	This study
HIVRT-K103N-ancestral	Fig. S28	UUUUACUUUUUUAACCCUGCGGGAUGUG	This study
HIVRT-K103N-derived	Fig. S28	UUGUACUUUUUUAACCCUGCGGGAUGUG	This study
HIVRT-V106M-ancestral	Fig. S28	GUUACUGAUUUUUUCUUUUUUAACCCUG	This study
HIVRT-V106M-derived	Fig. S28	GUCAUUGAUUUUUUCUUUUUUAACCCUG	This study
HIVRT-Y181C-	Fig. S28	GAUACAUAACUAUGUCUGGAU	This study

ancestral		UUUGUUU	
HIVRT-Y181C-derived	Fig. S28	GACACAUAACUAUGUCUGGAUUUUGUUU	This study
HIVRT-M184V-ancestral	Fig. S28	CAUGAAUUGAUAGAUAACUAUGUCUGGA	This study
HIVRT-M184V-derived	Fig. S28	CACGAAUUGAUAGAUAACUAUGUCUGGA	This study
HIVRT-G190A-ancestral	Fig. S28	AUCCAACAUACAAAUCAUCCAUGUAUUG	This study
HIVRT-G190A-derived	Fig. S28	AUGCAACAUACAAAUCAUCCAUGUAUUG	This study

Table S7. List of synthetic target sequences and RNA reporters used in this study.

All synthetic targets were ordered as gBlocks from IDT, and contain the 25 nucleotide T7 promoter sequence primer sequence (gaaatTAATACGACTCACTATAggg) at their 5' end. This allows for *in vitro* transcription of the gBlock, either before or after RPA amplification. Fluorescent reporters were ordered as HPLC-purified RNA oligonucleotides from IDT.

Name	**Used in**	**Sequence**	**Reference**
ZIKV_strt8924	Fig. 3, Fig. S19-S22	GAAATTAATACGACTCACTATAGGGGTGGAAGACTGCAGTGGA AGCTGTGAACGATCCAAGGTTCTGGGCTCTAGTGGACAAGGAA AGAGAGCACCACCTGAGAGGAGAGTGCCAGAGTTGTGTGTACA ACATGATGGGAAAAAGAGAAAAGAAACAAGGGGAATTTGGAAA GGCCAAGGGCAGCCGCGCCATCTGGTATATGTGGCTAGGGGCT AGATTTCTAGAGTTCGAAGCCCTTGGATTCTTGAACGAGGATC ACTGGATGGGGAGAGAGAACTCAGGAGGTGGTGTTGAAGGGCT GGGATTACAAAGACTCGGATATGTCCTAGAAGAGATGAGTCGC ATACCAGGAGGAAGGATGTATGCAGATGACACTGCTGGCTGGG ACACCCGCATCAGCAGGTTTGATCTGGAGAATGAAGCTCTAAT CACCAACCAAATGGAGAAAGGGCACAGGGCCTTGGCATT	This study
DENV_strt8284	Fig. 3, Fig. S19-S22	GAAATTAATACGACTCACTATAGGGATGGAACTCAGCAAAAGA GGCAGTGGAAGATGAACGGTTCTGGGACCTTGTGCACAGAGAG AGGGAGCTTCATAAACAAGGAAAATGTGCCACGTGTGTCTACA ACATGATGGGAAAGAGAGAGAAAAAATTAGGAGAGTTCGGAAA GGCAAAAGGAAGTCGCGCAATATGGTACATGTGGTTGGGAGCG CGCTTTTTAGAGTTTGAAGCCCTTGGTTTCATGAATGAAGATC ACTGGTTCAGCAGAGAGAATTCACTCAGTGGAGTGGAAGGAGA AGGACTCCACAAACTTGGATACATACTCAGAGACATATCAAAG ATTCCAGGGGGAAATATGTATGCAGATGACACAGCCGGATGGG ACACAAGAATAACAGAGGATGATCTTCAGAATGAGGCCAAAAT CACTGACATCATGGAACCTGAACATGCCCTATTGGCCAC	This study
WNV_strt8940	Fig. 3, Fig. S19-S22	GAAATTAATACGACTCACTATAGGGATGGAGGAGCGCCAGAGA AGCAGTTGAAGATCCAAAATTTTGGGAGATGGTGGATGAGGAG CGCGAGGCACATCTGCGGGGGGAATGTCACACTTGCATTTACA ACATGATGGGAAAGAGAGAGAAAAAACCCGGAGAGTTCGGAAA GGCCAAGGGAAGCAGAGCCATTTGGTTCATGTGGCTCGGAGCT CGCTTTCTGGAGTTCGAGGCTCTGGGTTTTCTCAATGAAGACC ACTGGCTTGGAAGAAAGAACTCAGGAGGAGGTGTCGAGGGCTT GGGCCTCCAAAAACTGGGTTACATCCTGCGTGAAGTTGGCACC CGGCCTGGGGGCAAGATCTATGCTGATGACACAGCTGGCTGGG ACACCCGCATCACGAGAGCTGACTTGGAAAATGAAGCTAAGGT GCTTGAGCTGCTTGATGGGGAACATCGGCGTCTTGCCAGGGCC ATCATTGAGCTCACCTA	This study

YFV_strt 8897	Fig. 3, Fig. S19-S22	GAAATTAATACGACTCACTATAGGGATGGAAGACAGCCAATGA AGCAGTCCAAGACCCCAAGTTTTGGGAGATGGTTGACGCTGAG CGCAAGCTCCATCAACAGGGGCGGTGCCAGTCTTGTGTCTATA ACATGATGGGAAAGAGAGAGAAAAAATTATCTGAATTTGGTAA AGCAAAAGGAAGCCGTGCCATCTGGTACATGTGGCTGGGGGCG CGTTTCCTCGAGTTTGAAGCTCTTGGGTTCCTGAATGAAGACC ACTGGGCATCCAGAGAGAATTCAGGAGGAGGTGTTGAAGGCAT AGGACTCCAATATCTAGGCTATGTAATCAAGGACCTATCCACC AAAGAAGGGGGAGGATTCTATGCTGATGACACAGCAGGATGGG ACACACGTATCACGGAAGCTGACCTAGACGATGAGCAGGAGAT CATGAGCTACATGAACGCTGAGCAGAGGAAACTGGCTTG	This study
DENV1_ strt10264	Fig. 3, Fig. S23-25	GAAATTAATACGACTCACTATAGGGCACTCTGGTAAGTCAACA CATTCACAAAACAAAGGAAAATAAGAAATCAAACAAGGCAAGA AGTCAGGCCGGATTAAGCCATAGTACGGTAAGAGCTATGCTGC CTGTGAGCCCCGTCTAAGGACGTAAAATGAAGTCAGGCCGGAA GCCACGGTTTGAGCAAACCGTGCTGCCTGTAGCTCCATCGTGG GGATGTAAAAACCCGGGAGGCTGCAACCCATGGAAGCTGTACG CATGGGGTAGCAGACTAGTGGTTAGAGGAGACCCCTCCCAAAA CACAACGCAGCAGCGGGGCCCAACACCAGGGGAAGCTGTACCC TGGTGGTAAGGACTAGAGGTTAGAGGAGACCCCCCGCACAACA ATAAACAGCATATTGACGCTGGGAGAGACCAGAGATCCTGCTG TCTCTACAGCATCATTCCAGGCACAGAACGCCAGAAAATGGAA TGGTGCTGTTGAATCAACAGGTTCT	This study
DENV2_ strt10251	Fig. 3, Fig. S23-25	GAAATTAATACGACTCACTATAGGGAGAGGCAGGAGTCCTGTG GTAGAAGGCAAAACTAACATGAAACAAGGCTAGAAGTCAGGTC GGATTAAGCCATAGTACGGAAAAAACTATGCTACCTGTGAGCC CCGTCCAAGGACGTTAAAAGAAGTCAGGCCATTACAAATGCCA TAGCTTGAGTAAACTGTGCAGCCTGTAGCTCCACCTGAGAAGG TGTAAAAAATCTGGGAGGCCACAAACCATGGAAGCTGTACGCA TGGCGTAGTGGACTAGCGGTTAGAGGAGACCCCTCCCTTACAA ATCGCAGCAACAATGGGGGCCCAAGGTGAGATGAAGCTGTAGT CTCACTGGAAGGACTAGAGGTTAGAGGAGACCCCCCCAAAACA AAAAACAGCATATTGACGCTGGGAAAGACCAGAGATCCTGCTG TCTCCTCAGCATCATTCCAGGCACAGAACGCCAGAAAATGGAA TGGTGCTGTTGAATCAACAGGTTCT	This study
DENV3_ strt10224	Fig. 3, Fig. S23-25	GAAATTAATACGACTCACTATAGGGAGAGATTCAGGAAGGAGG AGGAGTCAGAGGGAGCCATTTGGTAAAAGCAGGAGGCAAACTG TCAGGCCACCTTAAGCCACAGTACGGAAGAAGCTGTGCAGCCT GTGAGCCCCGTCCAAGGACGTTAAAAGAAGAAGTCAGGCCCAA AAGCCACGGTTTGAGCAAACCGTGCTGCCTGTAGCTCCGTCGT GGGGACGTAAAGCCTGGGAGGCTGCAAACCGTGGAAGCTGTAC GCACGGTGTAGCAGACTAGTGGTTAGAGGAGACCCCTCCCATG ACACAACGCAGCAGCGGGGCCCGAGCACTGAGGGAAGCTGTAC CTCCTGCAAAGGACTAGAGGTTATAGGAGACCCCCCGCAAACA AAAACAGCATATTGACGCTGGGAGAGACCAGAGATCCTGCTGT CTCCTCAGCATCATTCCAGGCACAGAACGCCAGAAAATGGAAT	This study

		GGTGCTGTTGAATCAACAGGTTCT	
DENV4_strt10181	Fig. 3, Fig. S23-25	GAAATTAATACGACTCACTATAGGGATCTGATCGGAAAAGAGG AATATGTGGATTACATGCCAGCCATGAAAAGATACAGCGCTCC TTTCGAGAGTGAAGGAGTTCTGTAATTGTTAACAACAAACACC AAAGGGACCATTGAAGTCAGGCCACTTGTGCCACGGCTTGAGC AAACCGTGCTGCCTGTAGCTCCGCCAATAATGGGAGGCGTAAA ATTCCCAGGGAGGCCATGCGCCACGGAAGCTGTACGCGTGGCA TATTGGACTAGCGGTTAGAGGAGACCCCTCCCATCACTGACAA AACGCAGCAAAAAAGGGGGCCCGAAGCCAGGAGGAAGCTGTAC TCCTGGTGGAAGGACTAGAGGTTAGAGGAGACCCCCCCAACAC AAAAACAGCATATTGACGCTGGGAAAGACCAGAGATCCTGCTG TCTCTGCAACATCAATCCAGGCACAGAGCGCCGCGAGATGGAT TGGTGTTGTTGATCCAACAGGTTCT	This study
DOMUSA 5249 ancestral target	Fig. 4	GAAATTAATACGACTCACTATAGGGTACCCAGCAGGAACTTCA GGATCTCCAATCCTAGACAAGTGTGGGAGAGTGATAGGACTTT ATGGCAATGGGGTCGTGATCAAAAATGGGAGTTATGTTAGTGC CATCACCCAAGGGAGGAGGGAGGAAGAGACTCCTGTTGAGTGC TTCGAGCCTTCGATGCTGAAGAAGAAGCAGCTAACTGTCTTAG ACTTGCATCCTGGAGCTGGGAAAACCAGGAGAGTTCTTCCCGA AATAGTCCGTGAAGCCATAAAAACAAGACTCCGTACTGTGATC TTAGCTCCAACCAGGGTTGTCGCTGCTGAAATGGAGGAAGCCC TTAGAGGGCTTCCAGTGCGTTATATGACAACAGCAGTCAATGT CACCCACTCTGGAACAGAAATCGTCGACTTAATGTGCC	This study
DOMUSA 5249 derived target	Fig. 4	GAAATTAATACGACTCACTATAGGGTACCCAGCAGGAACTTCA GGATCTCCAATCCTAGACAAGTGTGGGAGAGTGATAGGACTTT ATGGCAATGGGGTCGTGATCAAAAATGGGAGTTATGTTAGTGC CATCACCCAAGGGAGGAGGGAGGAAGAGACTCCTGTTGAGTGC TTCGAGCCTTCGATGCTGAAGAAGAAGCAGCTAACTGTCTTAG ACTTGCATCCTGGAGCTGGGAAAACCAGGAGAGTTCTTCCCGA AATAGTCCGTGAAGCTATAAAAACAAGACTCCGTACTGTGATC TTAGCTCCAACCAGGGTTGTCGCTGCTGAAATGGAGGAAGCCC TTAGAGGGCTTCCAGTGCGTTATATGACAACAGCAGTCAATGT CACCCACTCTGGAACAGAAATCGTCGACTTAATGTGCC	This study
USA 935 ancestral target	Fig. 4	GAAATTAATACGACTCACTATAGGGTGTGTACGGAACCTGCCA TCACAAAAAAGGTGAAGCACGGAGATCTAGAAGAGCTGTGACG CTCCCCTCCCATTCCACTAGGAAGCTGCAAACGCGGTCGCAAA CCTGGTTGGAATCAAGAGAATACACAAAGCACTTGATTAGAGT CGAAAATTGGATATTCAGGAACCCTGGCTTCGCGTTAGCAGCA GCTGCCATCGCTTGGCTTTTGGGAAGCTCAACGAGCCAAAAAG TCATATACTTGGTCATGATACTGCTGATTGCCCCGGCATACAG CATCAGGTGCATAGGAGTCAGCAATAGGGACTTTGTGGAAGGT	This study

		ATGTCAGGTGGGACTTGGGTTGATATTGTCTTGGAACATGGAG GTTGTGTCACCGTAATGGCACAGGACAAACCGACTGTC	
USA 935 derived target	Fig. 4	GAAATTAATACGACTCACTATAGGGTGTGTACGGAACCTGCCA TCACAAAAAAGGTGAAGCACGGAGATCTAGAAGAGCTGTGACG CTCCCCTCCCATTCCACTAGGAAGCTGCAAACGCGGTCGCAAA CCTGGTTGGAATCAAGAGAATACACAAAGCACTTGATTAGAGT CGAAAATTGGATATTCAGGAACCCTGGCTTCGCGTTAGCAGCA GCTGCCATCGCTTGGCTTTTGGGAAGCTCAACGAGCCAAAAAG TTATATACTTGGTCATGATACTGCTGATTGCCCCGGCATACAG CATCAGGTGCATAGGAGTCAGCAATAGGGACTTTGTGGAAGGT ATGTCAGGTGGGACTTGGGTTGATATTGTCTTGGAACATGGAG GTTGTGTCACCGTAATGGCACAGGACAAACCGACTGTC	This study
HND 2788 ancestral target	Fig. 4	GAAATTAATACGACTCACTATAGGGTCCCCCCGTAGATTGGCA GCAGCAGTCAAGCAAGCCTGGGAAGATGGTATCTGCGGGATCT CCTCTGTTTCAAGAATGGAAAACATCATGTGGAGATCAGTAGA AGGGGAGCTCAACGCAATCCTGGAAGAGAATGGAGTTCAACTG ACGGTCGTTGTGGGATCTGTAAAAAACCCCATGTGGGGAGGTC CACAGAGATTGCCCGTGCCTGTGAACGAGCTGCCCCACGGCTG GAAGGCTTGGGGGAAATCGCACTTCGTCAGAGCAGCAAAGACA AATAACAGCTTTGTCGTGGATGGTGACACACTGAAGGAATGCC CACTCAAACATAGAGCATGGAACAGCTTTCTTGTGGAGGATCA TGGGTTCGGGGTATTTCACACTAGTGTCTGGCTCAAGG	This study
HND 2788 derived target	Fig. 4	GAAATTAATACGACTCACTATAGGGTCCCCCCGTAGATTGGCA GCAGCAGTCAAGCAAGCCTGGGAAGATGGTATCTGCGGGATCT CCTCTGTTTCAAGAATGGAAAACATCATGTGGAGATCAGTAGA AGGGGAGCTCAACGCAATCCTGGAAGAGAATGGAGTTCAACTG ACGGTCGTTGTGGGATCTGTAAAAAACCCCATGTGGGGAGCTC CACAGAGATTGCCCGTGCCTGTGAACGAGCTGCCCCACGGCTG GAAGGCTTGGGGGAAATCGCACTTCGTCAGAGCAGCAAAGACA AATAACAGCTTTGTCGTGGATGGTGACACACTGAAGGAATGCC CACTCAAACATAGAGCATGGAACAGCTTTCTTGTGGAGGATCA TGGGTTCGGGGTATTTCACACTAGTGTCTGGCTCAAGG	This study
ZIKV mcep ancestral target	Fig. 4, Fig. S27	gaaatTAATACGACTCACTATAgggCTCATCAATAGATGGGGT TCAGTGGGGAAAAAAGAGGCTATGGAAATAATAAAGAAGTTCA AGAAAGATCTGGCTGCCATGCTGAGAATAATCAATGCTAGGAA GGAGAAGAAGAGACGGGGCGCAGATACTAGTGTCGGAATTGTT GGCCTCCTGCTGACCACAGCTATGGCAGCGGAGGTCACTAGAC GTGGGAGTGCATACTATATGTACTTGGACAGAAGCGATGCTGG GGAGGCCATATCTTTTCCAACCACATTGGGGATGAATAAGTGT TATATACAGATCATGGATCTTGGACACATGTGTGATGCCACCA TGAGCTATGAATGCCCTATGCTGGATGAGGGGGTGGAACCAGA TGACGTCGATTGTTGGTGCAACACGACGTCAACTTGGG	This study

ZIKV mcep derived target	Fig. 4, Fig. S27	gaaatTAATACGACTCACTATAgggCTCATCAATAGATGGGGT TCAGTGGGGAAAAAAGAGGCTATGGAAATAATAAAGAAGTTCA AGAAAGATCTGGCTGCCATGCTGAGAATAATCAATGCTAGGAA GGAGAAGAAGAGACGGGGCGCAGATACTAGTGTCGGAATTGTT GGCCTCCTGCTGACCACAGCTATGGCAGCGGAGGTCACTAGAC GTGGGAGTGCATACTATATGTACTTGGACAGAAACGATGCTGG GGAGGCCATATCTTTTCCAACCACATTGGGGATGAATAAGTGT TATATACAGATCATGGATCTTGGACACATGTGTGATGCCACCA TGAGCTATGAATGCCCTATGCTGGATGAGGGGGTGGAACCAGA TGACGTCGATTGTTGGTGCAACACGACGTCAACTTGGG	This study
HIVRT aa48-203 ancestral target	Fig. S28	gaaatTAATACGACTCACTATAgggTCAAAAATTGGGCCTGAA AATCCATACAATACTCCAGTATTTGCCATAAAGAAAAAAGACA GTACTAAATGGAGAAAATTAGTAGATTTCAGAGAACTTAATAA GAGAACTCAAGACTTCTGGGAAGTTCAATTAGGAATACCACAT CCCGCAGGGTTAAAAAAGAAAAAATCAGTAACAGTACTGGATG TGGGTGATGCATATTTTTCAGTTCCCTTAGATAAAGACTTCAG GAAGTATACTGCATTTACCATACCTAGTATAAACAATGAGACA CCAGGGATTAGATATCAGTACAATGTGCTTCCACAGGGATGGA AAGGATCACCAGCAATATTCCAAAGTAGCATGACAAAAATCTT AGAGCCTTTTAGAAAACAAAATCCAGACATAGTTATCTATCAA TACATGGATGATTTGTATGTAGGATCTGACTTAGAAATAGGGC AGCATAGAACAAAAATAGAG	This study
HIVRT aa48-203 K65R target	Fig. S28	gaaatTAATACGACTCACTATAgggTCAAAAATTGGGCCTGAA AATCCATACAATACTCCAGTATTTGCCATAAAGAGAAAAGACA GTACTAAATGGAGAAAATTAGTAGATTTCAGAGAACTTAATAA GAGAACTCAAGACTTCTGGGAAGTTCAATTAGGAATACCACAT CCCGCAGGGTTAAAAAAGAAAAAATCAGTAACAGTACTGGATG TGGGTGATGCATATTTTTCAGTTCCCTTAGATAAAGACTTCAG GAAGTATACTGCATTTACCATACCTAGTATAAACAATGAGACA CCAGGGATTAGATATCAGTACAATGTGCTTCCACAGGGATGGA AAGGATCACCAGCAATATTCCAAAGTAGCATGACAAAAATCTT AGAGCCTTTTAGAAAACAAAATCCAGACATAGTTATCTATCAA TACATGGATGATTTGTATGTAGGATCTGACTTAGAAATAGGGC AGCATAGAACAAAAATAGAG	This study
HIVRT aa48-203 K103N target	Fig. S28	gaaatTAATACGACTCACTATAgggTCAAAAATTGGGCCTGAA AATCCATACAATACTCCAGTATTTGCCATAAAGAAAAAAGACA GTACTAAATGGAGAAAATTAGTAGATTTCAGAGAACTTAATAA GAGAACTCAAGACTTCTGGGAAGTTCAATTAGGAATACCACAT CCCGCAGGGTTAAAAAAGAACAAATCAGTAACAGTACTGGATG TGGGTGATGCATATTTTTCAGTTCCCTTAGATAAAGACTTCAG GAAGTATACTGCATTTACCATACCTAGTATAAACAATGAGACA CCAGGGATTAGATATCAGTACAATGTGCTTCCACAGGGATGGA AAGGATCACCAGCAATATTCCAAAGTAGCATGACAAAAATCTT AGAGCCTTTTAGAAAACAAAATCCAGACATAGTTATCTATCAA TACATGGATGATTTGTATGTAGGATCTGACTTAGAAATAGGGC AGCATAGAACAAAAATAGAG	This study

HIVRT aa48-203 V106M target	Fig. S28	gaaatTAATACGACTCACTATAgggTCAAAAATTGGGCCTGAA AATCCATACAATACTCCAGTATTTGCCATAAAGAAAAAAGACA GTACTAAATGGAGAAAATTAGTAGATTTCAGAGAACTTAATAA GAGAACTCAAGACTTCTGGGAAGTTCAATTAGGAATACCACAT CCCGCAGGGTTAAAAAAGAAAAAATCAATGACAGTACTGGATG TGGGTGATGCATATTTTTCAGTTCCCTTAGATAAAGACTTCAG GAAGTATACTGCATTTACCATACCTAGTATAAACAATGAGACA CCAGGGATTAGATATCAGTACAATGTGCTTCCACAGGGATGGA AAGGATCACCAGCAATATTCCAAAGTAGCATGACAAAAATCTT AGAGCCTTTTAGAAAACAAAATCCAGACATAGTTATCTATCAA TACATGGATGATTTGTATGTAGGATCTGACTTAGAAATAGGGC AGCATAGAACAAAAATAGAG	This study
HIVRT aa48-203 Y181C target	Fig. S28	gaaatTAATACGACTCACTATAgggTCAAAAATTGGGCCTGAA AATCCATACAATACTCCAGTATTTGCCATAAAGAAAAAAGACA GTACTAAATGGAGAAAATTAGTAGATTTCAGAGAACTTAATAA GAGAACTCAAGACTTCTGGGAAGTTCAATTAGGAATACCACAT CCCGCAGGGTTAAAAAAGAAAAAATCAGTAACAGTACTGGATG TGGGTGATGCATATTTTTCAGTTCCCTTAGATAAAGACTTCAG GAAGTATACTGCATTTACCATACCTAGTATAAACAATGAGACA CCAGGGATTAGATATCAGTACAATGTGCTTCCACAGGGATGGA AAGGATCACCAGCAATATTCCAAAGTAGCATGACAAAAATCTT AGAGCCTTTTAGAAAACAAAATCCAGACATAGTTATCTGTCAA TACATGGATGATTTGTATGTAGGATCTGACTTAGAAATAGGGC AGCATAGAACAAAAATAGAG	This study
HIVRT aa48-203 M184V target	Fig. S28	gaaatTAATACGACTCACTATAgggTCAAAAATTGGGCCTGAA AATCCATACAATACTCCAGTATTTGCCATAAAGAAAAAAGACA GTACTAAATGGAGAAAATTAGTAGATTTCAGAGAACTTAATAA GAGAACTCAAGACTTCTGGGAAGTTCAATTAGGAATACCACAT CCCGCAGGGTTAAAAAAGAAAAAATCAGTAACAGTACTGGATG TGGGTGATGCATATTTTTCAGTTCCCTTAGATAAAGACTTCAG GAAGTATACTGCATTTACCATACCTAGTATAAACAATGAGACA CCAGGGATTAGATATCAGTACAATGTGCTTCCACAGGGATGGA AAGGATCACCAGCAATATTCCAAAGTAGCATGACAAAAATCTT AGAGCCTTTTAGAAAACAAAATCCAGACATAGTTATCTATCAA TACGTGGATGATTTGTATGTAGGATCTGACTTAGAAATAGGGC AGCATAGAACAAAAATAGAG	This study
HIVRT aa48-203 G190A target	Fig. S28	gaaatTAATACGACTCACTATAgggTCAAAAATTGGGCCTGAA AATCCATACAATACTCCAGTATTTGCCATAAAGAAAAAAGACA GTACTAAATGGAGAAAATTAGTAGATTTCAGAGAACTTAATAA GAGAACTCAAGACTTCTGGGAAGTTCAATTAGGAATACCACAT CCCGCAGGGTTAAAAAAGAAAAAATCAGTAACAGTACTGGATG TGGGTGATGCATATTTTTCAGTTCCCTTAGATAAAGACTTCAG GAAGTATACTGCATTTACCATACCTAGTATAAACAATGAGACA CCAGGGATTAGATATCAGTACAATGTGCTTCCACAGGGATGGA AAGGATCACCAGCAATATTCCAAAGTAGCATGACAAAAATCTT AGAGCCTTTTAGAAAACAAAATCCAGACATAGTTATCTATCAA	This study

		TACATGGATGATTTGTATGTAGCATCTGACTTAGAAATAGGGC AGCATAGAACAAAAATAGAG	
LF-polyU	Fig. 2, Fig. 4, Fig. S16	/56-FAM/UUUUUUUUUUUUU/3Bio/	This study

References

1. O. Faye *et al.*, One-step RT-PCR for detection of Zika virus. *J. Clin. Virol.* **43**, 96–101 (2008).

2. G. Paz-Bailey *et al.*, Persistence of Zika Virus in Body Fluids - Preliminary Report. *N. Engl. J. Med.* (2017), doi:10.1056/NEJMoa1613108.

3. H. C. Metsky *et al.*, Zika virus evolution and spread in the Americas. *Nature*. **546**, 411–415 (2017).

4. N. R. Faria *et al.*, Establishment and cryptic transmission of Zika virus in Brazil and the Americas. *Nature*. **546**, 406–410 (2017).

5. N. D. Grubaugh *et al.*, Genomic epidemiology reveals multiple introductions of Zika virus into the United States. *Nature*. **546**, 401–405 (2017).

6. O. Faye *et al.*, Quantitative real-time PCR detection of Zika virus and evaluation with field-caught mosquitoes. *Virol. J.* **10**, 311 (2013).

7. A.-C. Andries *et al.*, Value of Routine Dengue Diagnostic Tests in Urine and Saliva Specimens. *PLoS Negl. Trop. Dis.* **9**, e0004100 (2015).

8. J. J. Waggoner *et al.*, Comparison of the FDA-approved CDC DENV-1-4 real-time reverse transcription-PCR with a laboratory-developed assay for dengue virus detection and serotyping. *J. Clin. Microbiol.* **51**, 3418–3420 (2013).

9. I. Bosch *et al.*, Rapid antigen tests for dengue virus serotypes and Zika virus in patient serum. *Sci. Transl. Med.* **9** (2017), doi:10.1126/scitranslmed.aan1589.

10. A. Balmaseda *et al.*, Antibody-based assay discriminates Zika virus infection from other flaviviruses. *Proc. Natl. Acad. Sci. U. S. A.* **114**, 8384–8389 (2017).

11. L. Priyamvada *et al.*, Human antibody responses after dengue virus infection are highly cross-reactive to Zika virus. *Proc. Natl. Acad. Sci. U. S. A.* **113**, 7852–7857 (2016).

12. O. Piepenburg, C. H. Williams, D. L. Stemple, N. A. Armes, DNA detection using recombination proteins. *PLoS Biol.* **4**, e204 (2006).

13. J. S. Gootenberg *et al.*, Nucleic acid detection with CRISPR-Cas13a/C2c2. *Science*. **356**, 438–442 (2017).

14. O. O. Abudayyeh *et al.*, C2c2 is a single-component programmable RNA-guided RNA-targeting CRISPR effector. *Science*. **353**, aaf5573 (2016).

15. A. East-Seletsky *et al.*, Two distinct RNase activities of CRISPR-C2c2 enable guide-RNA processing and RNA detection. *Nature*. **538**, 270–273 (2016).

16. J. S. Gootenberg *et al.*, Multiplexed and portable nucleic acid detection platform with Cas13, Cas12a, and Csm6. *Science* (2018), doi:10.1126/science.aaq0179.

17. J. L. Weickmann, D. G. Glitz, Human ribonucleases. Quantitation of pancreatic-like enzymes in serum, urine, and organ preparations. *J. Biol. Chem.* **257**, 8705–8710 (1982).

18. R. Requena-Castro, M. Á. Reyes-López, R. E. Rodríguez-Reyna, P. Palma-Nicolás, V. Bocanegra-García, Molecular detection of mixed infections with multiple dengue virus serotypes in suspected dengue samples in Tamaulipas, Mexico. *Mem. Inst. Oswaldo Cruz*. **112**, 520–522 (2017).

19. S. Kim, A. Misra, SNP Genotyping: Technologies and Biomedical Applications. *Annu. Rev. Biomed. Eng.* **9**, 289–320 (2007).

20. L. Yuan *et al.*, A single mutation in the prM protein of Zika virus contributes to fetal microcephaly. *Science*, eaam7120 (2017).

21. S.-Y. Rhee *et al.*, Human immunodeficiency virus reverse transcriptase and protease sequence database. *Nucleic Acids Res.* **31**, 298–303 (2003).

22. Y. Du *et al.*, Coupling Sensitive Nucleic Acid Amplification with Commercial Pregnancy Test Strips. *Angew. Chem. Int. Ed Engl.* **56**, 992–996 (2017).

23. K. E. Eboigbodin, M. Brummer, T. Ojalehto, M. Hoser, Rapid molecular diagnostic test for Zika virus with low demands on sample preparation and instrumentation. *Diagn. Microbiol. Infect. Dis.* **86**, 369–371 (2016).

24. K. Pardee *et al.*, Rapid, Low-Cost Detection of Zika Virus Using Programmable Biomolecular Components. *Cell*. **165**, 1255–1266 (2016).

25. N. Chotiwan *et al.*, Rapid and specific detection of Asian- and African-lineage Zika viruses. *Sci. Transl. Med.* **9** (2017), doi:10.1126/scitranslmed.aag0538.

26. J. Van Ness, L. K. Van Ness, D. J. Galas, Isothermal reactions for the amplification of oligonucleotides. *Proceedings of the National Academy of Sciences*. **100**, 4504–4509 (2003).

27. C. B. Matranga *et al.*, Enhanced methods for unbiased deep sequencing of Lassa and Ebola RNA viruses from clinical and biological samples. *Genome Biol.* **15**, 519 (2014).

28. A. Abd El Wahed *et al.*, Recombinase Polymerase Amplification Assay for Rapid Diagnostics of Dengue Infection. *PLoS One*. **10**, e0129682 (2015).

29. C. L. Donald *et al.*, Full Genome Sequence and sfRNA Interferon Antagonist Activity of Zika Virus from Recife, Brazil. *PLoS Negl. Trop. Dis.* **10**, e0005048 (2016).

30. R. S. Lanciotti, A. J. Lambert, M. Holodniy, S. Saavedra, L. D. C. C. Signor, Phylogeny of Zika Virus in Western Hemisphere, 2015. *Emerg. Infect. Dis.* **22**, 933–935 (2016).

31. C. R. Lambeth, L. J. White, R. E. Johnston, A. M. de Silva, Flow cytometry-based assay for titrating dengue virus. *J. Clin. Microbiol.* **43**, 3267–3272 (2005).